An International Journal of Optimization and Control: Theories & Applications
ISSN: 2146-0957 eISSN: 2146-5703
Vol.16, No.3, pp.832-868 (2026)
https://doi.org/10.36922/IJOCTA026060022

REVIEW ARTICLE

A comprehensive review on fractional-order coronavirus models: Optimization of numerical results, control, applications, and future predictions

Kottakkaran Sooppy Nisar[1*], Muhammad Farman[2,3], Khadija Jamil[4], and Muhammad Kamran[5]

[1]Department of Mathematics, College of Science and Humanities, Prince Sattam bin Abdulaziz University, Al-Kharj, Saudi Arabia
[2]Department of Mathematics, Mathematics Research Center, Near East University, North Nicosia, Northern Cyprus, Turkey
[3]Research Center of Applied Mathematics, Khazar University, Baku, Azerbaijan
[4]International Center for Interdisciplinary Research in Sciences, The University of Lahore, Lahore, Punjab, Pakistan
[5]Research Institute of Business Analytics and SCM, College of Management, Shenzhen University, Shenzhen, Guangdong, China
n.sooppy@psau.edu.sa, farmanlink@gmail.com, khadijajamil675@gmail.com, kamrankfueit@gmail.com

ARTICLE INFO

Article History:
Received: February 3, 2026
Revised: March 14, 2026
Accepted: March 18, 2026
Published Online: May 14, 2026

Keywords:
COVID-19 model
Caputo fractional derivative
Hyers–Ulam–Rassias stability
Chaos
Numerical optimization control

AMS Classification 2010:
26A33; 34A08; 35H15; 34K50 47H10; 60H10

ABSTRACT

The outbreak of the COVID-19 pandemic has highlighted the need for advanced mathematical tools capable of accurately describing complex disease transmission dynamics. Fractional calculus has emerged as a powerful modeling framework due to its ability to incorporate memory effects and nonlocal behavior, which are intrinsic to infectious disease spread. This review provides a comparison of solutions obtained through the application of various fractional operators, including Caputo, Caputo–Fabrizio, Atangana–Baleanu derivative in Caputo sense, and fractal-fractional derivatives with power-law, exponential decay, and Mittag–Leffler memories. Key analytical properties such as positivity, boundedness, equilibrium analysis, basic reproduction number estimation, existence and uniqueness of solutions, Hyers–Ulam–Rassias stability, and chaos control are systematically discussed. The review further highlights the application of fractional models in capturing the effects of vaccination, quarantine, hospitalization, environmental transmission, and control interventions. By consolidating recent theoretical and applied advances, this work demonstrates the superiority of fractional-order models over classical integer-order approaches in reproducing real world COVID-19 dynamics. The presented review serves as a valuable reference for researchers and policymakers seeking robust and flexible modeling strategies for epidemic analysis and control.

1. Introduction

The COVID-19 pandemic has highlighted the need for accurate and reliable mathematical models to understand disease dynamics and guide public health interventions. Fractional calculus, which generalizes classical integer-order derivatives, provides a powerful framework for capturing memory-dependent and hereditary effects inherent in biological and epidemiological systems. By incorporating fractional-order derivatives, mathematical models can better reflect the influence of past states on current dynamics, offering more realistic predictions of

*Corresponding Author

infection spread, recovery, and hospitalization patterns. In this study, we focus on the application of fractional-order mathematical models in COVID-19, demonstrating how advanced analytical and numerical techniques can enhance our understanding of epidemic behavior and inform control strategies.

1.1. Background of COVID-19

In the first quarter of 2020, the spread of COVID-19 to several countries on every continent prompted the World Health Organization (WHO) to declare it a pandemic. The novel coronavirus has been shown to contain various mutations in multiple regions, which can cause various symptoms. Fever, dry cough, and fatigue are more frequent signs of illness than rash, diarrhea, loss of taste or smell, and sore throat. COVID-19 can spread through direct contact, indirect contact, droplet spray (from someone sneezing), short-range transmission, aerial transmission (via aerosol), and long-range transmission. In January 2020, the WHO announced a global health emergency due to the virus's rapid transmission among individuals and to several countries.[1] Consequently, the number of doctors and medical needs were insufficient to manage the increasing number of affected individuals.[2] Concerned about the rapid spread of the virus, many nations were racing to develop solutions to reduce fatalities among the growing number of patients.[3] The duration of the incubation phase varies from 1 to 14 days, with most cases being shorter than seven days.[4] Fever (37.5 °C) with a sore throat, cough, or both are typical signs of COVID-19.[5] Over 5,000 people have died from COVID-19 in China thus far, while over 10 million people have died worldwide. In addition to significantly affecting people's physical and emotional well-being, the pandemic has also had profound impacts on the global economy. Therefore, thorough investigation is essential to understand the effects of the COVID-19 pandemic on both mental health and economic stability.[6]

The COVID-19 pandemic has profoundly impacted human history, transforming the world in unprecedented ways and affecting nearly every aspect of society. Amid the numerous challenges and far-reaching consequences of the crisis, statistics have become increasingly vital as countries strive to understand and respond effectively to the pandemic. The review of the data focuses on the numerous facets of the COVID-19 pandemic, its impact on social dynamics, population health, the environment, and others, through an attentive analysis of data sources. The purpose of the given research is to provide a comprehensive image of the global implications of the pandemic by collecting and analyzing a number of data sources, focusing on the colossal scale of the effects and the experience gained when managing an event of this scale. Regarding the issue of public health, it proves the extent of morbidity, the cases of death, and the burden of health care systems in the world, which all plays a significant role in the lives of people. With regard to public health, it highlights the extent of morbidity, mortality rates, and the strain on healthcare systems worldwide, all of which play a significant role in people's lives.[7]

As the virus infected millions and spread to over 100 countries in the early stages of the pandemic, it appeared nearly unstoppable. It is important to contact current, trustworthy sources like the WHO for the most accurate and current information regarding COVID-19's impact in various nations, as a number of factors, such as developing variations, vaccination programs, and public health measures, can constantly change the status of the pandemic. To manage the spread of COVID-19 within the population, vaccines became available in January 2021.[9,10] In March 2023, the WHO permitted booster shots and primary series vaccination (i.e., using any two doses of vaccine) to counteract COVID-19 dynamics in the population. The duration of COVID-19 vaccination programs depends on vaccine effectiveness and the population's vulnerability to the disease. As of June 2023, an estimated 13 billion immunizations have been administered to stop the global spread of COVID-19. COVID-19 immunizations have avoided serious illness, hospitalization, and death, saving millions of lives; however COVID-19 immunization may not ensure complete recovery since recipients may still be able to spread the virus.[11,12]

1.2. Literature review

Over the past 20 years, advancements in medicine, access to healthcare, and hygiene have decreased the mortality and morbidity caused by viral diseases. However, infectious disease frequency remains high in low– and lower-middle-income nations, and neglected tropical diseases, tuberculosis, human immunodeficiency virus infection,[13] and malaria are still closely linked to death and morbidity. Khan et al.[14] used actual data from 1992 to 2020 to examine the spread of human immunodeficiency virus/acquired immunodeficiency syndrome in Pakistan using a mathematical model. In

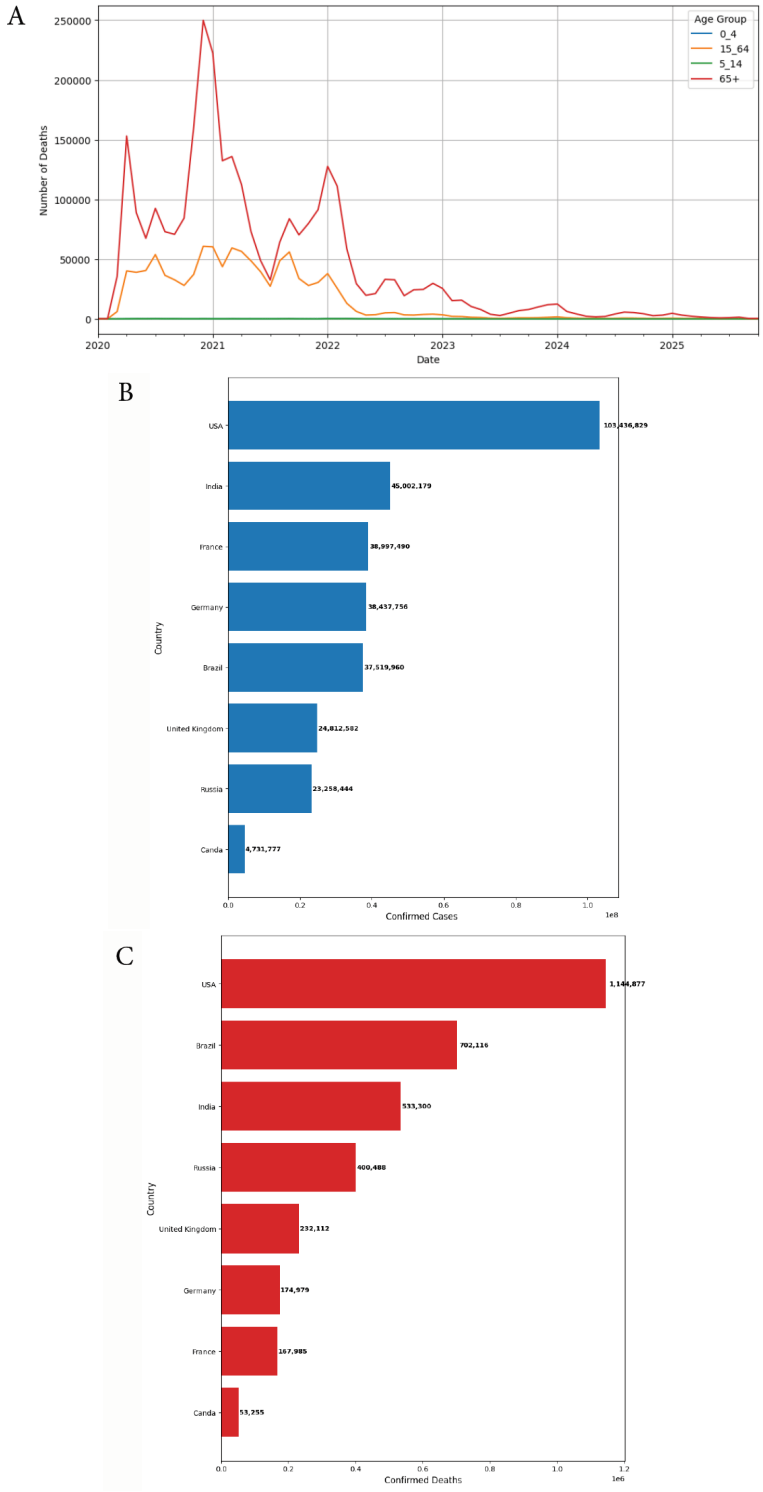

Figure 1. Distribution of COVID-19 cases worldwide. (A) Number of deaths from COVID-19 by four age groups in the years 2020 to 2025. The population aged 65 and above had the greatest mortality during the period, with steep peaks in the case of great infection waves in 2020–2021 and a slow decrease subsequently. Moderate changes were observed in the 15–64 age group with lower yet significant increases in the same wave patterns. Deaths in children in the age category 0–4 and 5–14 were very low and almost flat, showing that there is slight effect of mortality in the younger age groups. As a whole, the figure indicates the evident age-specific pattern of risks, according to which older adults are more susceptible to detrimental outcomes. (B) The confirmed number of cases in different countries. (C) The number of all confirmed deaths. According to data from January 2020 to December 4, 2023, the countries most affected by the COVID-19 pandemic were the United States of America, Brazil, and India.

the 21st century, infectious diseases continue to emerge and re-emerge, claiming lives worldwide.[15] Tuberculosis dynamics were analyzed using fractal-fractional derivatives,[16] and validated against real-world data for enhanced epidemic forecasting accuracy. Uar[17] employed fractal-fractional Caputo derivatives to model hepatitis B, while Ahmad et al.[18] calibrated with real Turkish data for precise disease insights, bifurcation, and theoretical analysis of a fractional-order hepatitis B model, accounting for varied chronic infection stages. Evirgen et al.[19] used a new mathematical model to examine the connection between heart attacks and the Omicron variant. Evirgen[20] investigated Nipah virus transmission dynamics through Caputo fractional derivatives. Naik et al.[21] explored fractional modeling of tumor carcinogenesis and macrophage interactions. In epidemiology, mathematical modeling has emerged as an essential tool for understanding the biological mechanism behind the dynamic transmission of SARS-CoV-2. The COVID-19 pandemic[22] highlighted the critical necessity for prompt and reliable infectious disease surveillance. Artificial intelligence (AI) can identify trends in massive datasets that may indicate the start of epidemics. In addition, a number of mathematical models were created to segment the entire population. Compartmental models are helpful tools for problem explanation because they can properly depict patterns of disease transmission. Many models have been developed to study the dynamics of disease transmission in a community.

1.2.1. Integer-order models

Olaniyi et al.[23] examined three categories of transmission in their thorough study of the dynamics of coronavirus disease transmission: hospitalized individuals, asymptomatic individuals, and symptomatic individuals. The model was calibrated using all of Nigeria's COVID-19 cases. Two time-dependent optimal controls were added in the study to prevent COVID-19 from spreading throughout the population. A solid mathematical model that included environmental influences on the dynamics of coronavirus disease transmission was created and examined by Asamoah et al.[24] Economic research identified the most economical strategy to prevent the maximum number of COVID-19 cases in the community. Using the concept of optimum control, the authors integrated control techniques into the constructed model. The authors concluded that the non-pharmaceutical strategy is the most economical means of preventing the greatest number of illnesses in the community among all the intervention options aiming for the same goal.

Kumar Rai et al.,[25] examined a mathematical model that considers the combined impact of environmental factors and vaccine efficacy on COVID-19 transmission. Similarly Das et al. ,[26] looked into how immigration and emigration affected COVID-19 transmission with respect to environmental conditions. Sharbayta et al.[27] highlighted the effect of double-dose vaccination on the dynamics of the coronavirus using a mathematical framework based on a system of ordinary differential equations. The study separated the developed model into two groups: the vaccination model and the no-vaccination model. Following a careful examination of the model, it was concluded that further vaccination efforts were required to effectively stop the threat of coronavirus infection. By including both isolated infected individuals getting treatment and isolated infected individuals not receiving treatment, Rois et al.[28] proposed a unique compartmental mathematical model. The study examined public education campaigns as a control approach to lower COVID-19 using optimal control theory. To comprehend how the alpha variant of the coronavirus propagated in Nigeria, Idisi et al.[29] developed a useful mathematical model. The effects of vaccination and a number of non-pharmaceutical strategies were considered to identify long-term answers to the current epidemic. Shen et al.[30] examined the optimal control analysis of a COVID-19 model with four control processes and vaccination.

Ullah and Khan[31] employed a mathematical model to examine the dynamics of the COVID-19 infection and employed several combinations of controls to determine the ideal approach for reducing the infection. Khan et al.[32] described the dynamics of COVID-19 infection during isolation and quarantine. In the work by Asamoah et al.[33] the coronavirus model's worldwide perspectives on Ghana's actual data and its economic analysis with environmental changes were examined. Péni et al. [34] developed a nonlinear predictive control model to treat the coronavirus infection. In the work of Matouk,[35] the use of drug resistance in coronavirus infection was proposed and studied. The spread probability of coronavirus infection in China has been computed and predicted by Sun et al.[36] To comprehend the dynamic analysis of the COVID-19-infected cases in the Kingdom of Saudi Arabia, Alshammari et al.

created a mathematical model and examined it.[37] A bacterial model for assessing coronavirus infection with vaccine availability was considered by Kumar et al.[38] The effectiveness of the vaccination was presented by Acuna-Zegarra[39] while a control analysis was performed by Asamoah et al.[40] In the work by Gatyeni et al.[41] the use of optimal control modeling to coronavirus infection using South African cases was examined. Using Malaysian infection cases, the effect of control intervention on coronavirus infection modeling was investigated by Abidemi et al.[42] Numerous additional important studies focused on coronavirus infection, its dynamical analysis, and infection controls. For further information on SARS-CoV-2 dynamical transmission in the population, readers should consult the following recent studies.[43,44]

1.2.2. Fractional-order models

Since the 19$^{\text{th}}$ century, the use of fractional calculus theory has grown significantly, encompassing, among other things, fractional dynamics, fractional geometry, and fractional differential equations. Fractional calculus methods and resources are used in practically every field of study and engineering.[45] For instance, chemical[46] and electrical engineering,[47] optical science, statistical and chemical physics,[48] bioengineering,[49] and other fields have many beneficial applications. Ahmad et al.[5051] developed a *Leptospirosis* model using fractal-fractional derivative in the Mittag–Leffler sense to investigate the dynamics of disease transmission incorporating human, animal, and bacterial populations.

In recent years, researchers have also created a number of fractional and fractal mathematical models of COVID-19. In, the work by Tajadodi et al.[52] the Atangana–Baleanu fractional derivative was used to address optimum control issues. Kouidere et al.[53] investigated the time series for the total number of confirmed cases of COVID-19, a novel coronavirus infection, for numerous African nations, and other studies[54,55] investigated the use of a fractional-order derivative for the COVID-19 model. Using the Caputo–Fabrizio operator, Farman et al. [56] created a COVID-19 Omicron variant model to study the dynamic transmission of the virus. Ma et al.[57] developed optimal control options for the mutant COVID-19 pandemic using fractional modeling.

Two-sided fractional modeling was used both qualitatively and statistically in COVID-19 multi-model selection and analysis.[58,59] The COVID-19 model consists of a system of fractional differential equations developed by researchers to capture the dynamics and effects of the disease. A thorough study of COVID-19 stochastic modeling with varying transmission rates and simulations based on actual statistical data from several has been conducted by Xu et al.[60] Rihan et al.[61] investigated the dynamics of a fractional-order asymptomatic COVID-19 model with several time delays, emphasizing stability and bifurcation analysis to comprehend the model's behavior under different circumstances. Moreover, the examines the dynamics and sensitivity of a fractional-order delay differential model for COVID-19 infection has been previously examined.[62] Padmavathi et al.[63] investigated the effect of the COVID-19 pandemic on mucus fluid. Environmental viral load was thought to be one of the primary ways that COVID-19 spreads, and it also has a significant impact on how the illness develops.

The model[64] with the effects of isolation, quarantine, and the environment on the dynamics of coronavirus transmission was reformulated using the Caputo derivative. In addition, a new fractional-order COVID-19 model that integrates lockdown intensity to more accurately capture real epidemic has also been presented.[65] Using fractional calculus, the model demonstrated improved flexibility in representing memory effects and behavioral changes during lockdown interventions. A fractional COVID-19[66] model with non-singular derivatives was developed to capture memory-driven infection dynamics more realistically. Numerical investigations reveal that varying the fractional order significantly alters epidemic trajectories, providing valuable insight for outbreak control. A delayed fractional order SEIHRM model[67] was formulated to capture the effects of memory and time lag in COVID-19 transmission alongside media influence. Results showed that media coverage and fractional dynamics jointly shaped infection trends, leading to more accurate predictions for behaviour of disease in Malaysia. Furthermore, innovative mathematical models were presented to describe the new coronavirus.[68,69] Several stochastic modeling approaches have been employed to study COVID 19 dynamics. A stochastic differential equation model was used to predict the spread of the novel coronavirus, examining long-term behavior, extinction probability, and sensitivity to random perturbations for more realistic forecasting amid uncertainties in transmission dynamics.[70] Another stochastic model captured random

variations in transmission to assess potential impacts on healthcare systems in India.[71] Additional studies investigated the role of random fluctuations in epidemic spread,[72] applied Bayesian vector autoregressions with stochastic volatility to account for data outliers and improve forecast robustness,[73] and analyzed infection dynamics using real-world data to provide insights into the inherent randomness of disease transmission.[74]

The use of fractional-order derivatives reveals the memory-dependent behavior of COVID-19 transmission, which cannot be captured by classical integer-order models. Unlike integer-order systems, the fractional framework incorporates the entire past history of infection, recovery, and hospitalization into the current dynamics. This allows the model to reflect non-exponential decay, hereditary immunity effects, and delayed responses more realistically. As a result, the fractional model uncovers richer dynamical patterns and more flexible epidemic trajectories that are not visible in integer-order formulations.

1.3. Motivation and contributions of study

The COVID-19 pandemic spread underscore the need for advanced mathematical models that can precisely represent the complex dynamics of COVID transmission. Memory effects and hereditary properties present in biological systems, especially in disease progression and recovery patterns, are frequently ignored by integer-order systems. By considering the memory-dependent aspect of disease transmission, the non-local operators of fractional calculus offer a more realistic framework for simulating such processes. The Caputo derivative offers substantial advantages for modeling biological systems, because it can handle initial conditions in a physically meaningful way. Despite these advantages, comprehensive studies integrating chaos control, advanced stability analysis, and efficient numerical schemes for fractional-order biological models are rare.[75] This research gap motivates the development of a comprehensive analytical and computational framework for a Caputo fractional-order SEAIHR COVID-19 model that bridges theoretical framework with practical applicability.

There are numerous contributions from this research. First, we expand the integer-order SEAIHR model into a fractional-order model that more realistically depicts the dynamics of COVID-19 transmission. Second, we ensure the well-posedness of the proposed model by verifying positivity and boundedness, and the presence of a single solution by employing fixed-point theory. Third, we examine the Hyers–Ulam stability that provides strong analytical surety for the behavior of the solution under variations. Fourth, we employ chaos control technique to govern the complex nonlinear dynamics that arise in epidemic models, improving the predictive power of the model. Fifth, to visualize the dynamical behavior of the system under different situations, we provided two-dimensional and three-dimensional phase space analysis. Sixth, we create an effective numerical approach based on Newton polynomials designed for the Caputo fractional-order system, providing better model simulation accuracy and computational efficiency. Collectively, these contributions improve the mathematical knowledge and practical application of fractional models, providing researchers and decision-makers better suggestions for assessing and predicting the dynamics of COVID-19 diseases.

The biological motivation is grounded in the fact that COVID-19 transmission involves memory effects, delayed progression, and inherited immunity patterns that classical integer-order models cannot fully capture. The use of the Caputo fractional operator allows the model to reflect how past infection history, hospitalization, and recovery influence current dynamics. By incorporating compartments such as exposed, asymptomatic, hospitalized, and recovered individuals, the model directly connects mathematical structure with realistic epidemic processes. The novelty of this work is based on the development of a comprehensive fractional-order SEAIHR COVID-19 framework that not only extends the classical integer-order SEAIHR COVID-19 model but also incorporates advanced analysis techniques such as Hyers–Ulam stability theory, chaos control, and a powerful numerical method based on Newton polynomials. This work is based on the fractional-order SEAIHR COVID-19 model because it is recognized that infectious diseases such as COVID-19 exhibit hereditary properties that cannot be captured by integer-order models. The use of fractional derivatives, particularly of the Caputo type, enables the SEAIHR COVID-19 model to incorporate the past history of the infections as well as the long-term immunity. This is particularly beneficial as the prediction accuracy of the SEAIHR COVID-19 model is enhanced, as is the understanding of the complex behavior of the SEAIHR COVID-19 model.

1.4. Structure of the article

The remaining part of the article is arranged as follows. In Section 2, we provide the basic concepts that will be used in the major part of the article. In Section 3, we review some existing COVID-19 models with several fractional and fractal fractional order derivatives. In Section 4, we provide a Caputo fractional-order derivative $SEAIHR$ model. In Section 5, we report the verification of positivity, boundedness, computed equilibrium points and reproductive number, prove the existence of a single solution and Hyers Ulam stability in Section 5. In Section 6, we perform chaos control analysis, while Section 7 generates the numerical scheme based on Newton polynomials. Section 8 provides the numerical solution of the studied model with various fractional orders. Lastly, Section 9 summarizes the research.

1.4.1. Basic concepts

In this section, we aim to provide some basic concepts that will be used in the main part of the article.

Definition 1. [76] *The Riemann–Liouville fractional integral of order $\sigma \in [0,1]$ for a function $Q(t)$ can be defined as follows:*

$$ {}^{RL}I^{\sigma}_{0,t}(\digamma(t)) = \frac{1}{\Gamma(\sigma)} \int_0^t (t-\vartheta)^{\sigma-1}[\digamma(\vartheta)]d\vartheta \quad (1)$$

The Caputo fractional derivative is very useful in applied sciences because it enables the inclusion of classical initial conditions represented in terms of integer-order derivatives. It is suitable for biological, epidemiological, and viscoelastic systems where past states significantly influence the current state because its power-law kernel naturally models long-term memory and hereditary effects.

Definition 2. [77] *For the function $\digamma(t)$, a Caputo derivative of fractional order $\sigma \in [0,1]$ can be expressed as follows:*

$$ {}^{C}D^{\sigma}_{t}(\digamma(t)) = \frac{1}{\Gamma(e-\sigma)} \int_0^t \frac{\digamma^{e}(\vartheta)}{(t-\vartheta)^{\sigma-n+1}}d\vartheta, \quad e = [\sigma]+1 \quad (2)$$

Definition 3. [77] *The corresponding Caputo integral operator with a fractional order $\sigma \in [0,1]$ is defined as follows:*

$$ {}^{C}I^{\sigma}_{t}(\digamma(t)) = \frac{1}{\Gamma(\sigma)} \int_0^t (t-\vartheta)^{\sigma-1}\digamma(\vartheta)d\vartheta \quad (3)$$

In the Caputo–Fabrizio derivative, a non-singular exponential kernel replaces the singular power-law kernel. This formulation is more suitable for systems with memory loss, fast decay processes, and numerical stability requirements because it avoids infinite memory effects and offers smoother dynamics.[78]

Definition 4. [79] *The Caputo–Fabrizio derivative for a function $\digamma(t)$ is defined as follows:*

$$ {}^{CF}D^{\sigma}_{0,t}(\digamma(t)) = \frac{\mathcal{W}(\sigma)}{1-\sigma} \int_0^t \sigma^{'}(\vartheta)\exp[\frac{\sigma(\vartheta-t)}{1-\sigma}]d\vartheta \quad (4)$$

where $\mathcal{W}(0) = 0 = \mathcal{W}(1)$, $\sigma > 0$ and $a-1 < \sigma < a,\ a \in \mathbb{N}$.

Definition 5. [79] *The Caputo–Fabrizio integral is defined as follows:*

$$ {}^{CF}I^{\sigma}_{0,t}(\digamma(t)) = \frac{2(1-\sigma)}{(2-\sigma)\mathcal{W}(\sigma)}\varsigma(t) + \frac{2\sigma}{(2-\sigma)\mathcal{W}(\sigma)} \int_0^t \digamma(\vartheta)d\vartheta \quad (5)$$

The ABC fractional derivative uses Mittag–Leffler kernel (FFM), which interpolates between properties of power-law and exponential memory. Because of its adaptability, the model can more accurately represent crossover dynamics and nonlocal impacts, particularly in biological and epidemiological processes with different time scales.

Definition 6. [80] *For a function $\digamma(t)$, the Antagana–Baleanu–Caputo derivative is defined as:*

$$ {}^{ABC}_{0}D^{\sigma}_{t}(\digamma(t)) = \frac{AB(\sigma)}{1-\sigma} \int_\sigma^t \frac{d}{d\vartheta}\digamma(\vartheta)\mathcal{E}_\sigma\left(-\sigma\frac{(t-\vartheta)^\sigma}{1-\sigma}\right)d\vartheta \quad (6)$$

where $AB(\sigma)$ is a normalization function and $\mathcal{E}_\sigma$ is the Mittag–Leffler function.

Remark 1. *The Laplace transformation for Equation (6) is defined as follows:*

$$ \mathcal{L}[{}^{ABC}_{0}D^{\sigma}_{t}(\digamma(t))](\mathcal{S}) = \frac{AB(\sigma)}{1-\sigma}\frac{\mathcal{S}^\sigma\mathcal{L}[\digamma(\vartheta)](\mathcal{S}) - \mathcal{S}^{\sigma-1}\digamma(0)}{\mathcal{S}^\sigma + \frac{\sigma}{1-\sigma}} \quad (7)$$

Using $\mathcal{ST}$ for Equation (6), we get

$$ \mathcal{ST}[{}^{ABC}_{0}D^{\sigma}_{t}(\digamma(t))](\mathcal{S}) = \frac{AB(\sigma)}{1-\sigma+\sigma\mathcal{S}^\sigma}[\mathcal{ST}\digamma(t) - \digamma(0)] \quad (8)$$

Definition 7. *The Atangana–Baleanu fractional integral of order σ for a function $\digamma(t)$ is expressed as*[81]*:*

$$ {}^{ABC}_{0}I^{\sigma}_{t}(\digamma(t)) = \frac{1-\sigma}{AB(\sigma)}\digamma(t) + \frac{\sigma}{AB(\sigma)\Gamma(\sigma)} \int_\sigma^t \digamma(\vartheta)(t-\vartheta)^{\sigma-1}d\vartheta \quad (9)$$

Definition 8. [82] *The MABC derivative of order* $0 < \sigma < 1$ *is defined by* $F \in \mathcal{L}^1(0, \mathbb{T})$*:*

$$
\begin{aligned}
&{}^{MABC}D_0^{\sigma} F(t) = \frac{AB(\sigma)}{1-\sigma} \\
&\Big[F(t) - \mathcal{E}_{\sigma}(-\eta_{\sigma} t^{\sigma}) F(0) - \eta_{\sigma} \\
&\int_0^t (t-\vartheta)^{\sigma-1} \mathcal{E}_{\sigma,\sigma}\left(-\eta_{\sigma}(t-\vartheta)^{\sigma}\right) F(\vartheta) d\vartheta\Big]
\end{aligned} \tag{10}
$$

where $\eta_{\sigma} = \frac{\sigma}{1-\sigma}$ and $AB(\sigma) = 1 - \sigma + \frac{\sigma}{\Gamma(\sigma)}$

The following is an expression for the Laplace transformation of the MABC derivative:

$$
\begin{aligned}
&\mathcal{L}\left\{{}^{MABC}D_t^{\sigma} F(t); u\right\} \\
&= \frac{AB(\sigma)}{(1-\sigma)} \frac{u^{\sigma}\mathcal{L}\left\{F(t); u\right\} - u^{\sigma-1}F(0)}{u^{\sigma} + \eta_{\sigma}}, \quad \left|\frac{\eta_{\sigma}}{u^{\sigma}}\right| < 1
\end{aligned} \tag{11}
$$

Systems with excellent long-term memory and scale invariance use the power-law based fractal-fractional derivative. By adding spatial or temporal fractality, it improves fractional models and produces more realistic simulations of complex systems.

Definition 9. *Let* $F(t)$ *be a function that may or may not be differentiable. With* $0 < \sigma \leq 1$ *and* $0 < \varpi \leq 1$,[83] *defines the fractal fractional derivative with a power-law kernel as follows for a given fractal dimension* ϖ *and fractional order* σ*.*

$$
\begin{aligned}
&{}^{FFP}D_{0,t}^{\sigma,\varpi}(F(t)) = \\
&\frac{1}{\Gamma(a-\sigma)} \frac{d}{dt^{\varpi}} \int_0^t (t-\vartheta)^{a-\sigma-1} F(\vartheta) d\vartheta
\end{aligned} \tag{12}
$$

$$
\frac{d}{d\vartheta^{\varpi}} F(\vartheta) = lim_{t\to\vartheta} \frac{F(t) - F(\vartheta)}{t^{\varpi} - \vartheta^{\varpi}} \tag{13}
$$

The associated integral is defined as:

$$
\begin{aligned}
&{}^{FFP}I_{0,t}^{\sigma,\varpi}(F(t)) = \frac{1}{\Gamma(\sigma)} \\
&\int_0^t (t-\vartheta)^{\sigma-1} \vartheta^{1-\varpi} F(\vartheta) d\vartheta
\end{aligned} \tag{14}
$$

Fractal-fractional derivative with exponential kernel explains the memory effects and the fractal nature of complex media simultaneously. It is helpful for simulating biological tissues, porous structures, and heterogeneous environments where geometric irregularity and memory loss are important factors.[84]

Definition 10. *Let* $F(t)$ *be a possibly non-differentiable function. With* $0 < \sigma \leq 1$ *and* $0 < \varpi \leq 1$,[83] *presents the fractal fractional derivative with an exponential decay kernel for a fractal dimension* ϖ *and a fractional order* σ*.*

$$
\begin{aligned}
&{}^{FFE}D_{0,t}^{\sigma,\varpi}(F(t)) \\
&= \frac{\mathcal{W}(\sigma)}{\Gamma(a-\sigma)} \frac{d}{dt^{\varpi}} \\
&\int_0^t \exp[-\frac{\sigma}{1-\sigma}(t-\vartheta)^{a-\sigma-1}] F(\vartheta) d\vartheta
\end{aligned} \tag{15}
$$

where $\sigma > 0$, $\varpi \leq a \in \mathbb{N}$, and $\mathcal{W}(0) = \mathcal{M}(1) = 1$.

The associated integral is given by:

$$
\begin{aligned}
&{}^{FFE}D_{0,t}^{\sigma,\varpi}(F(t)) = \frac{\varpi(1-\sigma)t^{\varpi-1}F(t)}{\mathcal{W}(\sigma)} \\
&+\frac{\sigma\varpi}{\mathcal{W}(\sigma)} \int_0^t \vartheta^{\sigma-1} F(\vartheta) d\vartheta
\end{aligned} \tag{16}
$$

The fractal-fractional operator with FFM is very good option to use in case of anomalous diffusion and multi-scale dynamics. This method unifies nonlocal temporal effects, fractal geometry, and long-range dependence.[85]

Definition 11. [80]

$$
\begin{aligned}
&{}^{FFM}D_{0,t}^{\sigma,\varpi}(F(t)) = \\
&\frac{AB(\sigma)}{1-\sigma} \frac{d}{dt^{\varpi}} \int_0^t \mathcal{E}_{\sigma}[-\frac{\sigma}{1-\sigma}(t-\vartheta)^{\sigma}] F(\vartheta) d\vartheta
\end{aligned} \tag{17}
$$

where $0 < \sigma,\ \varpi \leq 1$ *and* $AB(\sigma) = 1 - \sigma + \frac{\sigma}{\Gamma(\sigma)}$.

The associated integral is provided by:

$$
\begin{aligned}
&{}^{FFM}D_{0,t}^{\sigma,\varpi}(F(t)) = \frac{\varpi(1-\sigma)t^{\upsilon-1}F(t)}{AB(\sigma)} + \\
&\frac{\sigma\varpi}{AB(\sigma)} \int_0^t \vartheta^{\sigma-1}(t-\vartheta) F(\vartheta) d\vartheta
\end{aligned} \tag{18}
$$

Definition 12. *In,*[86] *a general non-fractional differential operator, widely known as the proportional or conformable operator, was formulated as follows:*

$$
{}^{P}D_t^{\sigma} F(t) = \mathcal{K}_1(\sigma, t) F(t) + \mathcal{K}_0(\sigma, t) F'(t) \tag{19}
$$

where $\mathcal{K}_0(\sigma, t) = \sigma t^{1-\sigma}, \quad \mathcal{K}_1(\sigma, t) = (1-\sigma)t^{\sigma}$ (20)

Moreover, $\mathcal{K}_0$ *and* $\mathcal{K}_1$ *are functions of* t *and* $\sigma \in [0, 1]$ *that satisfy the following conditions for all* $t \in \mathbb{R}$*:*

$$
\begin{aligned}
&\lim_{\sigma\to 0^+} \mathcal{K}_0(\sigma, t) = 0, \quad \lim_{\sigma\to 1^-} \mathcal{K}_0(\sigma, t) = 1, \\
&\mathcal{K}_0(\sigma, t) \neq 0, \quad \sigma \in (0, 1] \\
&\lim_{\sigma\to 0^+} \mathcal{K}_1(\sigma, t) = 1, \ \lim_{\sigma\to 1^-} \mathcal{K}_1(\sigma, t) = 0, \\
&\mathcal{K}_1(\sigma, t) \neq 0, \quad \sigma \in [0, 1)
\end{aligned} \tag{21}
$$

Moreover, a particularly important special case arises when the functions $\mathcal{K}_0$ *and* $\mathcal{K}_1$ *are constant with respect to* t *and depend only on* σ*. This operator is known as the constant proportional operator and is defined as follows:*

$$
{}^{CP}D_t^{\sigma} F(t) = \mathcal{K}_1(\sigma) F(t) + \mathcal{K}_0(\sigma) F'(t) \tag{22}
$$

Definition 13. *In,*[87] *a hybrid fractional operator, referred to as the proportional Caputo operator,*

was introduced by combining the proportional operator with the Caputo fractional derivative.

$$
\begin{aligned}
{}_0^{PC}D_t^{\sigma}F(t) &= \frac{1}{\Gamma(1-\sigma)} \\
&\int_0^t \Big(\mathcal{K}_1(\sigma,\vartheta)F(\vartheta) + \mathcal{K}_0(\sigma,\vartheta)\mathcal{Z}'(\vartheta)\Big) \\
&(t-\vartheta)^{-\sigma}d\vartheta \\
&= {}_0^{RL}I_t^{1-\sigma}\Big[\mathcal{K}_1(\sigma,t)F(t) + \mathcal{K}_0(\mu,t)\mathcal{Z}'(t)\Big]
\end{aligned} \tag{23}
$$

When $\mathcal{K}_0$ and $\mathcal{K}_1$ are independent of t, the operator ${}^{CP}D_{\sigma}$ is known as the constant proportional Caputo operator, which is defined as follows:

$$
\begin{aligned}
{}_0^{CPC}D_t^{\sigma}F(t) &= \frac{1}{\Gamma(1-\sigma)} \\
&\int_0^t \Big(\mathcal{K}_1(\sigma)F(\vartheta) + \mathcal{K}_0(\sigma)F'(\vartheta)\Big) \\
&(t-\vartheta)^{-\sigma}d\vartheta \\
&= \mathcal{K}_1(\sigma)\ {}_0^{RL}I_t^{1-\sigma}F(t) + \\
&\mathcal{K}_0(\sigma)\ {}_0^{C}D_t^{\mu}\mathcal{Z}(t)
\end{aligned} \tag{24}
$$

The constant proportional Caputo derivative becomes very good in controlling the impact of memory effects by adding proportionality to the fractional operator. This derivative increases the flexibility of the model and helps adjust system responses without changing the fractional order.[88]

Definition 14. [89] *If $\sigma \in (0,1]$ and $\varpi \in \mathbb{C}$, $Re(\varpi) > 0$, then, the left-sided generalized proportional integral of order ϖ for the function F is defined as:*

$${}_cI_t^{\sigma,\varpi}F(t) = \frac{1}{\sigma^{\varpi}\Gamma(\varpi)}\int_c^t e^{\frac{\sigma-1}{\sigma}(t-\vartheta)}(t-\vartheta)^{\varpi-1}F(\vartheta)d\vartheta \tag{25}$$

2. Description of fractional-order COVID-19 models

2.1. SAIVR model with Caputo derivative

An important field of epidemiological research is the study of the dynamics of COVID-19 viral transmission and control in human populations. The existence and uniqueness of solutions, stability analysis using the Hyers–Ulam–Rassias criterion, and the identification of steady states are among the features of a compartmental model that are examined.[76] Utilizing the non-local property of the Caputo fractional-order derivative, which is derived from a power-law type kernel, this study reformulates an existing integer-order SAIVR model into the Caputo sense. The model generalizes the classical framework by incorporating a fractional-order parameter, allowing for the analysis of system dynamics across a continuum of orders. The following set of equations represents the Caputo-type SAIVR model:

$$
\begin{aligned}
&{}^{C}D_t^{\sigma}S(t) = -\beta_1 I\tfrac{S}{N} - \rho_1 A\tfrac{S}{N} - \delta\tfrac{S}{N} + (1-\lambda)\,\varepsilon V,\\
&{}^{C}D_t^{\sigma}A(t) = \rho_1 A\tfrac{S}{N} + \beta_2 I\tfrac{S}{N} + \eta A\tfrac{V}{N} - \gamma A,\\
&{}^{C}D_t^{\sigma}I(t) = \beta_1 I\tfrac{S}{N} + \rho_2 A\tfrac{S}{N} + \upsilon I\tfrac{V}{N} - \gamma I,\\
&{}^{C}D_t^{\sigma}V(t) = \delta\tfrac{S}{N} - \eta A\tfrac{V}{N} - \upsilon I\tfrac{V}{N} - \varepsilon V,\\
&{}^{C}D_t^{\sigma}R(t) = \gamma I + \gamma A + \lambda\varepsilon V
\end{aligned} \tag{26}
$$

By including memory effects and genetic traits, this fractional generalization aims to provide a more accurate representation of the COVID-19 pandemic dynamics than the conventional integer-order model.

2.2. SLII$_q$RP model with Caputo derivative

The dynamics of COVID-19 virus transmission and control in human populations are an important area of epidemiological research.[90] The features of a complex compartmental model are examined in this paper, including the boundedness and uniqueness of its solution, and a comprehensive stability analysis of both endemic and disease-free equilibria. Utilizing the non-local property of the Caputo fractional-order derivative, this study formulates a novel model that segments the population into susceptible (S), latent (L), clinically infected (I), quarantined (I_q), hospitalized (I_h), and recovered (R) individuals, with an additional compartment for the pathogen load in the environment (P). By adding a fractional-order parameter, the model expands on a traditional integer-order framework, enabling a more detailed examination of the memory-dependent dynamics of the system.

The Caputo model is given by the following system of equations:

$$
\begin{aligned}
&{}^{C}D_t^{\sigma}S(t) = \varsigma - \tfrac{\beta S}{N}(I+\theta L) - \Theta S - \pi SP,\\
&{}^{C}D_t^{\sigma}L(t) = \tfrac{\beta S}{N}(I+\theta L) - (\Theta+\omega+\tau)L + \pi SP,\\
&{}^{C}D_t^{\sigma}I(t) = \tau L - (\Theta+\delta+\Theta_i+\varphi+\alpha+\phi)I,\\
&{}^{C}D_t^{\sigma}I_q(t) = \phi I - (\Theta+\varepsilon+\Theta_q)I_q,\\
&{}^{C}D_t^{\sigma}R(t) = \delta I + \omega L + \lambda I_h + \varepsilon I_q - \Theta R,\\
&{}^{C}D_t^{\sigma}P(t) = \alpha I - \Theta_p P
\end{aligned} \tag{27}
$$

The primary objective of this fractional generalization is to account for memory effects and provide a more accurate representation of the COVID-19 pandemic dynamics, particularly by assessing the impact of hospitalization and quarantine, as well as the importance of environmental pathogen load. The boundedness

of the solution is shown using the Laplace transform on a fractional Gronwall's inequality, and its existence and uniqueness are confirmed using fixed-point theory. The stability analysis using Lyapunov functions shows that the disease-free equilibrium is globally asymptotically stable when $R_0 < 1$, whereas the endemic equilibrium is stable when $R_0 > 1$.

2.3. Optimal control model with Caputo–Fabrizio operator

Hanif et al.[91] suggested an optimal control Caputo Fabrizio-based fractional order model to determine the best measures for quarantine and hospitalization.

The suggested SEQIHR model is given by:

$$\begin{aligned}
{}^{CF}D^{\sigma}S(t) &= \lambda - [\beta E + \Pi I + \beta_3 H]S - \mu S,\\
{}^{CF}D^{\sigma}E(t) &= [\beta E + \Pi I + \beta_3 H]S - (\alpha + \mu + \rho)E,\\
{}^{CF}D^{\sigma}Q(t) &= \rho E - (\Xi + q_3 + \mu + d_3)Q,\\
{}^{CF}D^{\sigma}I(t) &= \alpha E - (\xi + \gamma + \mu + \Psi)I,\\
{}^{CF}D^{\sigma}H(t) &= \Xi Q + \xi I - (\omega + \mu + \Phi)H,\\
{}^{CF}D^{\sigma}R(t) &= \gamma I + q_3 Q + \omega H - \mu R.
\end{aligned}$$

where $S(t)$ is the class of vulnerable humans, $E(t)$ is the class of exposed humans, $I(t)$ is group of infected humans, and $H(t)$ is the class of hospitalized humans, $R(t)$ is the group of humans recovered from COVID disease. λ is the inflow rate vulnerable humans, μ is the natural mortality rate for all groups of humans, β, Π and β_3 are the contact rates with exposed, infected, and hospitalized humans, α is the rate at which exposed humans develop symptoms to become infected, ξ is the rate at which infected humans move to come hospitalized class, γ is the rate at which infected humans are recovered, ω is the rate at which hospitalized humans are recovered, and $\Psi, and \Phi$ are the death rates of infected and hospitalized humans. ρ is the quarantine rate of exposed humans, Ξ is the hospitalization rate of quarantined humans, q_3 is the recovery rate of quarantined humans, and d_3 is the mortality rate of quarantined humans due to COVID disease.

With the control variables $u_1(t)$ and $u_2(t)$, the above $SEQIHR$ COVID model takes the form:

$$\begin{aligned}
{}^{CF}D^{\sigma}S(t) &= \lambda - [\beta E + \Pi I + \beta_3 H]S - \mu S,\\
{}^{CF}D^{\sigma}E(t) &= [\beta E + \Pi I + \beta_3 H]S - (\alpha + \mu + u_1(t))E,\\
{}^{CF}D^{\sigma}Q(t) &= u_1(t)E - (\Xi + q_3 + \mu + d_3)Q,\\
{}^{CF}D^{\sigma}I(t) &= \alpha E - (u_2(t) + \gamma + \mu + \Psi)I,\\
{}^{CF}D^{\sigma}H(t) &= \Xi Q + u_2(t)I - (\omega + \mu + d_2)H,\\
{}^{CF}D^{\sigma}R(t) &= \gamma I + q_3 Q + \omega H - \mu R
\end{aligned}$$

2.4. JEIR model with Caputo–Fabrizio derivative

This work introduces a fractional-order COVID-19 epidemic model using the Caputo–Fabrizio fractional derivative,[92] which more closely captures the memory effects and non-local dynamics observed in actual disease transmission than traditional integer-order models. It offers a precise and effective analytical solution to the nonlinear system by utilizing the innovative fractional homotopy perturbation transform method (FHPTM), providing a greater understanding of the intricate behavior of the pandemic.

$$\begin{aligned}
{}^{CF}D_t^{\sigma}J(t) &= a - KI(t)J(t)(1 + \alpha I(t)) - d_o J(t),\\
{}^{CF}D_t^{\sigma}E(t) &= KI(t)J(t)(1 + \alpha I(t)) - (d_o + \tau)E(t),\\
{}^{CF}D_t^{\sigma}I(t) &= b + \alpha E(t) - (\mu + d_o + \beta)I(t),\\
{}^{CF}D_t^{\sigma}R(t) &= \beta I(t) - d_o R(t)
\end{aligned} \tag{28}$$

The Caputo–Fabrizio operator, used for the JEIR model, employs a non-singular exponential kernel suitable for systems with memory loss and fast decay, offering smoother dynamics and better numerical stability compared to the Caputo operator's singular power-law kernel for long-term memory. In contrast to the Atangana–Baleanu–Caputo operator's FFM, which interpolates between power-law and exponential behaviors for crossover dynamics, Caputo–Fabrizio avoids complex functions, simplifying computations while capturing nonlocal effects in fading-memory epidemiological scenarios like COVID-19.

The work rigorously proves the stability and convergence of the proposed method through fixed-point theory, enhancing its reliability for predictive purposes. Numerical simulations for different fractional orders clearly demonstrate how the disease dynamics (susceptible, exposed, infected, and recovered populations) depend on the fractional parameter, giving policymakers a more flexible and realistic tool. Ultimately, this research advances mathematical epidemiology by showing that fractional calculus can significantly improve the understanding and forecasting of rapidly spreading infectious diseases like COVID-19.

2.5. SVEAIR model with ABC derivative

Converting an integer-order epidemiological model to a fractional-order model has many significant advantages.[93] Because fractional models account for memory and genetic elements, they are better able to represent the long-term dynamics and history-dependent behavior of

infectious illnesses. Compared to integer-order models, which suggest that the future state depends entirely on the present, fractional models account for the influence of previous states, producing more precise and realistic explanations of disease progression.

$$
\begin{aligned}
&{}^{ABC}D^{\sigma}S(t) = \Pi - \tfrac{(a_1 I + a_2 A)S}{N} - (\varkappa + \omega)\, S + \\
&\Theta R + \theta V, \\
&{}^{ABC}D^{\sigma}V(t) = \omega S - (1-\psi)\, \tfrac{(a_1 I + a_2 A)V}{N} - \\
&(\theta + \varkappa)\, V, \\
&{}^{ABC}D^{\sigma}E(t) = \tfrac{(a_1 I + a_2 A)S}{N} + (1-\psi) \\
&\tfrac{(a_1 I + a_2 A)V}{N} - (\delta + \varkappa)\, E, \\
&{}^{ABC}D^{\sigma}A(t) = \delta q E - (\varkappa + \rho_1)\, A, \\
&{}^{ABC}D_t^{\sigma}I(t) = -(d + \varkappa + \rho)\, I + \delta\,(1-q)\, E, \\
&{}^{ABC}D^{\sigma}R(t) = \rho_1 A + \rho I - (\varkappa + \Theta)\, R
\end{aligned}
\tag{29}
$$

In complex systems like COVID-19, where disease transmission is impacted by delayed reactions and long-term immunological effects, this improved modeling capabilities frequently leads to better forecasts and better fitting of real-world data.

2.6. SIQPD model with fractal-fractional power-law operator

Sinan and Alharthi[94] suggested a COVID-19 fractal-fractional model to investigate the biological effects of COVID-19 on humans. The authors established global and local stability, computed the reproductive number, utilized the Castillo–Chavez method to verify the presence of bifurcation, performed sensitivity analysis, and formulated the optimal control system characterized using Pontryagin's maximum principle. The model simulation was performed with numerous fractal-fractional orders by employing the Adam Bashforth method.

The system of equations suggested by[94] is given by:

$$
\begin{aligned}
{}^{FFP}D^{\sigma,\varpi}S(t) &= v - \xi S(t) - \frac{\theta S(t) I(t)}{1 + \phi I(t)}, \\
{}^{FFP}D^{\sigma,\varpi}I(t) &= \frac{\theta S(t) I(t)}{1 + \phi I(t)} - \\
&\quad (\xi + \chi + \Theta + \varrho_1) I(t), \\
{}^{FFP}D^{\sigma,\varpi}Q(t) &= \Theta I(t) - (\xi + \varsigma + \varrho_2) Q(t), \\
{}^{FFP}D^{\sigma,\varpi}P(t) &= \chi I(t) + \varsigma Q(t) - \xi P(t), \\
{}^{FFP}D^{\sigma,\varpi}D_{IQ}(t) &= \varrho_1 I(t) + \varrho_2 Q(t)
\end{aligned}
$$

where $S(t)$ is the group of susceptible humans, $I(t)$ is the group of infected humans, $Q(t)$ is the class of quarantined humans, and $P(t)$ is the class of protected humans, $D_{IQ}(t)$ is the group of humans containing dead persons from infected and quarantined groups. v is the inflow rate, ξ is the rate of natural mortality, θ is the rate of transmission, ω is the proportion of psychological effects on humans, χ is the rate of recovery of infected humans, ς is the rate at which recovery humans are isolated, Θ denotes the rate at which the exposed humans develop symptoms to become period, ϱ_1 is the death rate of infected humans due to COVID, and ϱ_2 is the death rate of quarantined humans due to COVID.

2.7. SEIVR model with fractal-fractional power-law operator

Kubra and Ali[95] examined the impact of vaccination on the spread of COVID-19 using a five-compartment model in the sense of a fractal-fractional derivative incorporating a power-law kernel. The suggested model was also fitted with real data for Pakistan. The model underwent comprehensive qualitative and quantitative analysis by computing the equilibrium points, reproduction number, verification of the feasible region, proof of the presence of a single solution, validation of stability, and identification of sensitive parameters.

$$
{}^{FFP}D^{\sigma,\varpi}S(t) = \Pi - \omega E S - (\varphi + \varsigma) S, \tag{30}
$$

$$
{}^{FFP}D^{\sigma,\varpi}E(t) = \omega S E + \gamma V E - \beta I E - (\upsilon + \varsigma) E, \tag{31}
$$

$$
{}^{FFP}D^{\sigma,\varpi}I(t) = \beta I E - (r + \delta + \varsigma) I, \tag{32}
$$

$$
{}^{FFP}D^{\sigma,\varpi}V(t) = \varphi S - \gamma E V - \varsigma V, \tag{33}
$$

$$
{}^{FFP}D^{\sigma,\varpi}R(t) = rI + \upsilon E - \varsigma R, \tag{34}
$$

where $S(t)$ is the class of susceptible humans, $E(t)$ is the group of exposed humans, $I(t)$ is the class of infected humans, $V(t)$ is the class of vaccinated humans, $R(t)$ is the group of recovered humans.

Π is the inflow rate of vulnerable humans, ω is the rate at which vulnerable humans move to exposed humans, and φ is the rate at which vulnerable humans are vaccinated to boost their immunity, β is the rate at which exposed humans develop symptoms to move in infected class, γ is the rate of COVID exposure of vaccinated humans, r is the rate of recovery of infected humans, ς is the natural mortality rate for all classes of humans, υ is the rate of recovery of exposed humans, and δ is the mortality rate of infected humans due to COVID.

2.8. $SQEI_hIRP$ model with Mittag-Leffler kernel operator

By replicating complicated dynamics, memory effects, and non-local behaviors that are present in epidemic processes, the fractal-fractional operator has been applied to enhance the simulation of the COVID-19 pandemic.[96] The complex linkages and temporal dependencies seen in the spread of diseases like COVID-19 may be better represented by the model with the use of this operator. This method provides a more comprehensive framework for researching epidemic dynamics, improving forecast accuracy, and providing valuable information for creating efficient preventative and control measures. An expanded fractal-fractional formulation using FFM transforms this classical model into a fractional-order framework, enabling the assessment of societal impact and dynamic transmission factors.

$$
\begin{aligned}
&{}^{FFM}D_{0,t}^{\sigma,\varpi}S(t) = A + mR - \tfrac{\alpha SP}{1+\omega_1 P} - \tfrac{\beta S(I+I_h)}{1+\omega_2(I+I_h)} - \kappa S,\\
&{}^{FFM}D_{0,t}^{\sigma,\varpi}Q(t) = \tfrac{\alpha SP}{1+\omega_1 P} + \tfrac{\beta S(I+I_h)}{1+\omega_2(I+I_h)} - \gamma_1 Q - \kappa Q,\\
&{}^{FFM}D_{0,t}^{\sigma,\varpi}E(t) = \tfrac{(1-\varsigma)\alpha SP}{1+\omega_1 P} + \tfrac{(1-\varsigma)\beta S(I+I_h)}{1+\omega_2(I+I_h)} -\\
&\theta\gamma_2 E - (1-\varsigma)\,\theta\gamma_2 E - \kappa E,\\
&{}^{FFM}D_{0,t}^{\sigma,\varpi}I_h(t) = \gamma_1 Q + (1-\theta)\,\gamma_2 E - \eta_1 I_h -\\
&(\kappa+\delta)\,I_h,\\
&{}^{FFM}D_{0,t}^{\sigma,\varpi}I(t) = \theta\gamma_2 E - \eta_2 I - (\kappa+\delta)\,I,\\
&{}^{FFM}D_{0,t}^{\sigma,\varpi}R(t) = \eta_1 I_h + \eta_2 I - mR - \kappa R,\\
&{}^{FFM}D_{0,t}^{\sigma,\varpi}P(t) = \mu I - \kappa P
\end{aligned}
\tag{35}
$$

2.9. Sugar and diabetes coinfection $SDEICR$ model with Mittag–Leffler kernel operator

Farman et al.[97] suggested a coinfection fractal fractional model in the Mittag-Leffler sense to study the impact of COVID-19 on diabetic patients.

$$
\begin{aligned}
&{}_0^{FFM}D_t^{\sigma,\varpi}S(t) = \Omega - \beta\left(\frac{I+C}{N}\right)S - (\Theta+\lambda)S,\\
&{}_0^{FFM}D_t^{\sigma,\varpi}D(t) = \lambda S + \gamma_1 C - \beta\left(\frac{I+C}{N}\right)D -\\
&\qquad(\delta_2+\Theta)D,\\
&{}_0^{FFM}D_t^{\sigma,\varpi}E(t) = \beta\left(\frac{I+C}{N}\right)S + \beta\left(\frac{I+C}{N}\right)D -\\
&\qquad(\phi+\Theta)E,\\
&{}_0^{FFM}D_t^{\sigma,\varpi}I(t) = \alpha\phi E - (\delta+\Theta+\gamma)I,\\
&{}_0^{FFM}D_t^{\sigma,\varpi}C(t) = (1-\alpha)\phi E - (\delta_1+\Theta)C,\\
&{}_0^{FFM}D_t^{\sigma,\varpi}R(t) = \gamma I - \Theta R
\end{aligned}
\tag{36}
$$

where $S(t)$ is the group of vulnerable humans from COVID, $D(t)$ is the group of the humans vulnerable with diabetes, $E(t)$ is the class of exposed humans (infected but not yet infectious), $I(t)$ is the class of humans infected with COVID-19 without diabetes, $C(t)$ is the group of humans infected with COVID and diabetes, and $R(t)$ is the class of humans recovered from disease. Ω is the inflow rate of vulnerable humans, β is the rate of transmission of COVID, Θ is the rate of natural mortality, λ is the rate of infection of vulnerable humans from diabetes, γ_1 is the rate of recovery of humans infected with diabetes, δ_2 is the mortality induced rate due to diabetes, ϕ is the rate at which exposed humans move to infected humans. α is the fraction of moving exposed humans to infected humans without diabetes, δ is the COVID-induced mortality rate, γ is the rate at which diabetes patients recover, and δ_1 is the rate at which patients of COVID-19 and diabetes die.

2.10. SEQ I_A I_S H V R model with different kernels

Kubra et al.[98] investigated a COVID model incorporating hospitalized and vaccinated humans by considering in the sense of fractal fractional Caputo Fabrizio, Caputo and Atanganaâ–Baleanu derivatives. The authors computed the reproduction number, ensured local and global stability of equilibrium points, and verified the presence of a single solution. In addition, the model was fitted with the real data of Pakistan.

The suggested $SEQI_AI_SHVR$ model is given by:

$$
\begin{aligned}
&{}^{FF}D^{\sigma,\varpi}S(t) = \Pi - \omega ES - (\Xi + m + \varphi),\\
&{}^{FF}D^{\sigma,\varpi}E(t) = \rho EV + \omega SE - (\gamma + \upsilon_1 + \upsilon_2 + \alpha + \varphi),\\
&{}^{FF}D^{\sigma,\varpi}Q(t) = \Xi S + \gamma E - (\Xi_1 + \Xi_2 + \varphi),\\
&{}^{FF}D^{\sigma,\varpi}I_A(t) = \upsilon_1 E + \digamma V + \Xi_1 Q - (\Lambda_1 + \delta + \varphi),\\
&{}^{FF}D^{\sigma,\varpi}I_S(t) = \upsilon_2 E + \Xi_2 Q - h_1 H I_S - (\Lambda_2 + \varphi)I_S,\\
&{}^{FF}D^{\sigma,\varpi}H(t) = h_1 H I_S - (h_2 + \Lambda_3 + \delta + \varphi)H,\\
&{}^{FF}D^{\sigma,\varpi}V(t) = mS + h_2 H - \rho EV - (\digamma + \varphi)V,\\
&{}^{FF}D^{\sigma,\varpi}R(t) = \alpha E + \Lambda_1 I_A + \Lambda_2 I_S + \Lambda_3 H - \varphi R
\end{aligned}
\tag{37}
$$

where $S(t)$ denotes the susceptible humans, $E(t)$ represents the exposed humans, $Q(t)$ is the class of quarantined humans, $I_A(t)$ is group of asymptomatically infected humans, $I_S(t)$ is class of symptomatically infected humans, $H(t)$ is consists of hospitalized humans, $V(t)$ is the population of vaccinated human population, and $R(t)$ is recovered human's population. Π is the recruitment rate through birth or immigration, and φ is the natural mortality rate, and δ is

the mortality rate due to COVID disease, Ξ is the quarantine rate of susceptible humans, ω is the rate of transmission from susceptible to exposed humans, γ is the quarantine rate of exposed humans, m is vaccination rate of susceptible humans, Ξ_2 is the rate at which quarantined humans move to symptomatically infected humans, p is the rate at which vaccinated humans become exposed, Ξ_1 rate at which quarantined humans move towards asymptomatically infected humans, α is the rate of recovery of exposed humans, Λ_1 is the rate of recovery of asymptomatic infected humans, Λ_2 is the rate of recovery of symptomatic infected humans, Λ_3 is rate of recovery of hospitalized humans, h_1 is the rate of hospitalization of symptomatically infected humans, h_2 is the rate of booster dose administration to hospitalized humans, Θ_1 is the rate at which exposed humans move to asymptomatic infected humans, Θ_2 is the rate at which exposed humans move to symptomatic infected humans, and $\digamma$ is the rate at which vaccinated humans move to asymptomatic infected humans.

2.11. SIV model with piecewise ABC operator

The piecewise ABC derivative allows different fractional behaviors in different time intervals. This is particularly important for modeling systems with regime switching, control interventions, or stage-wise dynamics, such as epidemic control strategies or treatment phases.

Shah and Abdeljawad[99] examined the influence of vaccination in a susceptible, infected, and vaccinated COVID model with piecewise ABC derivatives and stochastic noise terms. The authors also calculated the strength number and simulated the model with real data.

$$
\begin{aligned}
{}_0^{PABC}D^{\sigma}S(t) &= (1-\mu)a - \frac{\beta SI}{N} - \mu S,\\
{}_0^{PABC}D^{\sigma}I(t) &= \frac{\beta SI}{N} + \frac{\alpha VI}{N} - (\Theta+\rho+\gamma)I,\\
{}_0^{PABC}D^{\sigma}V(t) &= \mu a - \frac{\alpha VI}{N} - \Theta V + \gamma I
\end{aligned}
$$

Fractional stochastic models combine nonlocal memory effects with random perturbations, providing a more realistic representation of real systems subject to environmental noise and uncertainty. Such models are essential for capturing randomness, robustness, and uncertainty propagation in biological, epidemiological, financial, and engineering systems.

In Equation XXX 38, $S(t)$ denotes the number of vulnerable humans at any time t, $I(t)$ is the number of infected humans, $V(t)$ is the number of vaccinated humans, a is the inflow rate, β is the rate at which vulnerable humans are infected, α is the rate at which vaccinated humans are infected rate, μ is the rate of vaccination rate, Θ is the natural mortality rate, ρ is the death rate of infected humans due to COVID, γ is the rate at which infected humans get immunity and recover, and θ_i is the intensity of noise, $B_i(t)$ is the Brownian motion process.

2.12. Caputo fractional $SITR$ model with lockdown

Adel et al.[100] suggested an SITR model composed of susceptible, infected, treated, and recovered humans, with the susceptible population further divided into susceptible with lockdown and susceptible without lockdown. Laplace Adomian decomposition technique was used to find a solution, in addition to a comparison with real data was demonstrated showing agreement between the obtained data and the Laplace Adomian technique solution. The authors demonstrated that if quarantine is implemented, COVID can be controlled easily.

The suggested model by[100] is given below:

$$
\begin{aligned}
D^{\sigma}S_1(t) &= \Theta - \beta S_1(t)I(t) - \Psi_1 S_1(t)R(t) - \gamma S_1(t) +\\
&\quad \Pi_1 I(t) + \Pi_2 T(t) + \Lambda_1 S_2(t),\\
D^{\sigma}S_2(t) &= \Psi_1 S_1(t)R(t) - \gamma S_2(t) - \Lambda_1 S_2(t),\\
D^{\sigma}I(t) &= \beta S_1(t)I(t) - \Pi_1 I(t) - \xi_1 I(t) - \gamma I(t) -\\
&\quad \Psi_2 I(t)R(t) + \Lambda_2 T(t),\\
D^{\sigma}T(t) &= \Psi_2 I(t)R(t) - \gamma T(t) - \Lambda_2 T(t) -\\
&\quad \Pi_2 T(t) - \xi_2 T(t),\\
D^{\sigma}R(t) &= \theta I(t) - \psi R(t)
\end{aligned}
$$

where $S_1(t)$ is the class of vulnerable humans not under lockdown, $S_2(t)$ is the class of susceptible humans under lockdown, $I(t)$ is the class of infected humans not under lockdown, and $T(t)$ is the class of isolated or treated infected humans under lockdown, $R(t)$ is the group of recovered humans. Θ is the inflow rate, β is the rate of infection due to human-to-human contact, Π_1 is the rate of recovery of infected humans, Π_2 is the rate of recovery for treated humans, Ψ_1 is the rate at which vulnerable humans are under lockdown, Ψ_2 is the rate at whcih infected humans are under lockdown, ξ_1 is the rate at whcih infected humans die due to COVID disease, ξ_2 is the rate at which treated humans die due to COVID, γ is the natural mortality rate of humans, Λ_1 is the rate at which vulnerable humans under lockdown

move to vulnerable humans not under lockdown. Λ_2 is the rate at which infected humans under lowckdown move to infected humans class not under lockdown, θ is the rate at which humans obtain immunity and got recovered, and ψ is the relapse rate of recovered humans.

3. Description of the COVID-19 model

Akanni et al.[101] presented an integer-order COVID-19 model and verified the non-negativity and boundedness of solutions, proved the stability of endemic equilibrium points using Lyapunov function, when the reproductive number is greater than 1. The impact of parameters on the spread of COVID -19 is illustrated through the partial rank correlation coefficient. Six control interventions were also used to lower the burden of COVID -19 in society.

In this study, we aim to apply the Caputo operator on the existing model from Akanni et al.[101] and provide positivity and boundedness in the Caputo sense, Chaos control analysis, existence of a unique solution in the Caputo sense, and Hyers–Ulam stability. We applied the caputo operator on the SEAIHR because of its excellent ability to capture memory effects and inherited characteristics present in biological processes. The Caputo operator is perfect for modeling epidemiological systems where historical states affect current transmission and recovery rates because, unlike integer-order derivatives, it takes into account the full history of system dynamics through its non-local kernel. Mathematically, the Caputo derivative directly corresponds with quantifiable epidemiological data by considering usual initial conditions with an obvious physical explanation.[102] The fractional order σ is a key parameter representing various population interactions, different latency intervals, and non-exponential delay durations in disease progression. Additionally, when modeling constant recruitment and mortality rates, the Caputo formulation ensures biological realism by maintaining dimensional consistency and producing zero derivative for constant functions. Together, these benefits improve the model's capacity to accurately depict complex disease dynamics while maintaining mathematical feasibility for analysis and simulation.

The COVID - 19 $SEAIHR$ mathematical model with Caputo operator is represented in the following form:

$$\begin{aligned}
&{}^{C}D_t^{\sigma} S(t) = \Lambda - (\lambda + \mu)\, S,\\
&{}^{C}D_t^{\sigma} E(t) = \lambda S - (\varepsilon + \theta + \mu)\, E,\\
&{}^{C}D_t^{\sigma} A(t) = \varepsilon E - (\mu + \psi + \phi + \kappa)\, A,\\
&{}^{C}D_t^{\sigma} I(t) = \theta E + \psi A - (\mu + \delta + \omega)\, I,\\
&{}^{C}D_t^{\sigma} H(t) = \phi A + \omega I - (\mu + \delta + \rho)\, H,\\
&{}^{C}D_t^{\sigma} R(t) = \kappa A + \rho H - \mu R,
\end{aligned} \tag{38}$$

where

$$\lambda = \frac{\beta\,(I + \eta A)}{N},$$

in terms of the non-negative initial conditions. **Figure 2** describes the pictorial representation of the relationship between parameters and compartments, while **Table 1** includes parameter values and descriptions of parameters from.[101]

4. Qualitative and quantitative analysis of the COVID-19 model

4.1. Positivity of the model

To preserve biological significance in epidemiological modeling, the solutions must stay non-negative. This property prevents non-physical negative values from being attained by population compartments. The following theorem verifies the positivity of solutions for the suggested Caputo fractional-order SEAIHR model.

Theorem 1. *With non-negative initial conditions and positive biological parameters, all solutions for the Caputo fractional-order system given in Equation (38) stay non-negative for all values of time.*

Proof: We start by defining the norm: $\|Y\| = \sup_{t\in D_Y} |Y(t)|$, where D_Y denotes the domain of $Y(t)$. Considering the expression for susceptible humans from the model, we have:

$$\begin{aligned}
{}^{C}D_t^{\sigma} S(t) &= \Lambda - \left(\frac{\beta(I + \eta A)}{N} + \mu\right) S\\
&\geq -\left(\frac{\beta(\|I\| + \eta\|A\|)}{N} + \mu\right) S\\
&= -\left(\frac{\beta(\|I\| + \eta\|A\|)}{N} + \mu\right) S
\end{aligned}$$

where $N(t)$ denotes the total population over the time domain.

$$\begin{aligned}
{}^{C}D_t^{\sigma} E(t) &= \lambda S - (\varepsilon + \theta + \mu)E,\\
&\geq -(\varepsilon + \theta + \mu)E(t),\\
&= -(\varepsilon + \theta + \mu)E(t)
\end{aligned}$$

$$\begin{aligned}
{}^{C}D_t^{\sigma} A(t) &= \varepsilon E - (\mu + \psi + \phi + \kappa)A,\\
&\geq -(\mu + \psi + \phi + \kappa)A(t),\\
&= -(\mu + \psi + \phi + \kappa)A(t)
\end{aligned}$$

Table 1. The values and explanation of the COVID-19 model parameters

Parameters	Description[101]	Values
Λ	Inflow rate of humans	1500
η	Rate of reduced infectiousness of acutely infected individuals	0.4
ϵ	Rate at which exposed humans become acutely infected	0.18
ψ	Rate at which acutely infected humans move to infected humans	0.1
κ	Rate of recovery of acutely infected humans through natural immune system or hospitalization	0.13978
ω	Rate at which infected humans move to hospitalized class	0.0264
β	Rate at which susceptible humans contact with acutely infected and infectious humans to become exposed	0.492
μ	Rate of natural death rate	0.01277
θ	Rate at which exposed humans move to infected humans	0.02
ϕ	Rate at which acutely infected humans move to hospitalized humans	0.083
δ	Rate of COVID-19 induced mortality	0.036
ρ	Recovery rate of hospitalized individuals	0.096

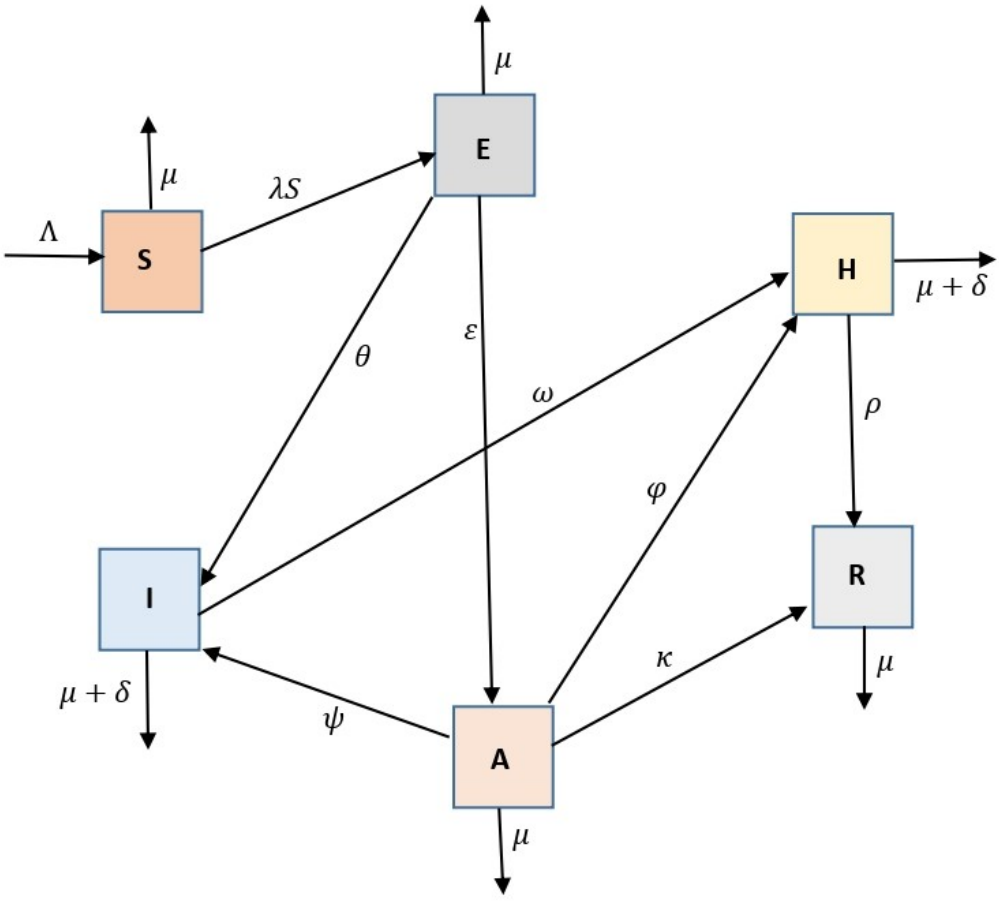

Figure 2. Flow chart of the studied SEAIHR COVID-19 model

$$
\begin{aligned}
{}^{C}D_t^{\sigma} I(t) &= \theta E + \psi A - (\mu + \delta + \omega) I, \\
&\geq -(\mu + \delta + \omega) I(t), \\
&\quad -(\mu + \delta + \omega) I(t)
\end{aligned}
$$

$$
\begin{aligned}
{}^{C}D_t^{\sigma} H(t) &= \phi A + \omega I - (\mu + \delta + \rho) H, \\
&\geq -(\mu + \delta + \rho) H(t), \\
&= -(\mu + \delta + \rho) H(t).
\end{aligned}
$$

$$
\begin{aligned}
{}^{C}D_t^{\sigma} R(t) &= \kappa A + \rho H - \mu R, \\
&\geq -\mu R(t), \\
&= -\mu R(t)
\end{aligned}
$$

We derive the following lower bounds for each compartment by using the properties of the Mittag–Leffler function and the fractional comparison principle:

$$
\begin{aligned}
S(t) &\geq S(0) E_{\sigma}\left(- \left(\frac{\beta(\|I\| + \eta \|A\|)}{N} + \mu \right) t^{\sigma} \right) \\
E(t) &\geq E(0) E_{\sigma}\left(-(\varepsilon + \theta + \mu) t^{\sigma} \right) \\
A(t) &\geq A(0) E_{\sigma}\left(-(\mu + \psi + \phi + \kappa) t^{\sigma} \right) \\
I(t) &\geq I(0) E_{\sigma}\left(-(\mu + \delta + \omega) t^{\sigma} \right) \\
H(t) &\geq H(0) E_{\sigma}\left(-(\mu + \delta + \rho) t^{\sigma} \right) \\
R(t) &\geq R(0) E_{\sigma}\left(-\mu t^{\sigma} \right)
\end{aligned}
$$

Since the Mittag–Leffler function $E_{\sigma}(-ct^{\sigma})$ is strictly positive for all $c > 0$, $\sigma \in (0, 1]$, and $t \geq 0$, all compartments remained non-negative for non-negative initial states. This completes the proof of non-negativity.

This theorem is biologically important because it ensures the non-negativity of each population in each compartment, which is important for biological feasible solution. The ability of the model to accurately depict the dynamics of diseases in the real world depends on this feature.

4.2. Boundedness of solution

In dynamical systems theory, a region is called positively invariant if, once the system enters it, it stays there. This area serves as the biologically feasible domain for epidemiological models, where all compartments stay within reasonable bounds, and the whole population stays bounded.

Theorem 2. *For the suggested fractional-order SEAIHR model (38), the closed set* $\Omega = \left\{ (S, E, A, I, H, R) \in \mathbb{R}_+^6 : N(t) \leq \frac{\Lambda}{\mu} \right\}$ *stays positively invariant.*

Proof:

$$
\begin{aligned}
{}^{C}D_t^{\sigma} S(t) &= \Lambda \geq 0, \\
{}^{C}D_t^{\sigma} E(t) &= \lambda S \geq 0, \\
{}^{C}D_t^{\sigma} A(t) &= \varepsilon E \geq 0, \\
{}^{C}D_t^{\sigma} I(t) &= \theta E + \psi A \geq 0, \\
{}^{C}D_t^{\sigma} H(t) &= \phi A + \omega I \geq 0, \\
{}^{C}D_t^{\sigma} R(t) &= \kappa A + \rho H \geq 0
\end{aligned}
\tag{39}
$$

Let

$$N(t) = S(t) + E(t) + A(t) + I(t) + H(t) + R(t)$$

be the total population of the system. Summing all equations of Equation (38), we obtain

$$
\begin{aligned}
{}^{C}D_t^{\sigma} N(t) &= \Lambda - \mu S - \mu E - \mu A - \mu I - \mu H - \mu R - \delta I - \delta H \\
{}^{C}D_t^{\sigma} N(t) &= \Lambda - \mu(S + E + A + I + H + R) - \delta(I(t) + H(t)) \\
{}^{C}D_t^{\sigma} N(t) &= \Lambda - \mu N(t) - \delta(I(t) + H(t))
\end{aligned}
$$

Since $I(t) \geq 0$ and $H(t) \geq 0$, it follows that

$${}^{C}D_t^{\sigma} N(t) \leq \Lambda - \mu N(t)$$

Consider the fractional differential equation

$${}^{C}D_t^{\sigma} N(t) = \Lambda - \mu N(t).$$

$$
\begin{aligned}
{}^{C}D_t^{\sigma} N(t) &= \Lambda - \mu N - \delta(I + H) \\
&\leq \Lambda - \mu N
\end{aligned}
$$

Using the Laplace transform and the properties of the Mittag–Leffler function,

$$\mathcal{L}\{N(t)\} = N(s) \leq \frac{\Lambda}{s(s^{\sigma} + \mu)} + N(0) \frac{s^{\sigma - 1}}{s^{\sigma} + \mu}$$

where $\mathcal{L}\{\cdot\}$ denotes the Laplace transform. Applying the inverse Laplace transform on both sides, the result is:

$$
\begin{aligned}
N(t) &\leq N(0) E_{\sigma}(-\mu t^{\sigma}) + \int_0^t \Lambda \tau^{\sigma - 1} E_{\sigma,\sigma}(-\mu \tau^{\sigma}) d\tau \\
&\leq N(0) E_{\sigma}(-\mu t^{\sigma}) + \int_0^t \Lambda \tau^{\sigma - 1} \sum_{k=0}^{\infty} \frac{(-\mu)^k \tau^{k\sigma}}{\Gamma(k\sigma + \sigma)} d\tau \\
&= N(0) E_{\sigma}(-\mu t^{\sigma}) + \Lambda \sum_{k=0}^{\infty} \frac{(-\mu)^k}{\Gamma(k\sigma + \sigma)} \int_0^t \tau^{k\sigma + \sigma - 1} d\tau \\
&= N(0) E_{\sigma}(-\mu t^{\sigma}) + \Lambda \sum_{k=0}^{\infty} \frac{(-\mu)^k t^{k\sigma + \sigma}}{\Gamma(k\sigma + \sigma + 1)} \\
&= \frac{\Lambda}{\mu} + E_{\sigma}(-\mu t^{\sigma}) \left(N(0) - \frac{\Lambda}{\mu} \right)
\end{aligned}
$$

where $E_{\sigma}(z)$ denotes the one-parameter Mittag–Leffler function and $E_{\sigma,\sigma}(z)$ represents the two-parameter Mittag–Leffler function. This expression makes it clear that for any $t > 0$, $N(t) \leq \frac{\Lambda}{\mu}$ if $N(0) \leq \frac{\Lambda}{\mu}$. Consequently, under the dynamics of the Caputo fractional derivative system, the closed set Ω is positively invariant.

Biologically, this invariant region denotes the carrying capacity of the population, which is established by the equilibrium between the natural mortality rate μ and the recruitment rate Λ. The greatest sustainable population size in the absence of disease-induced mortality is represented by the upper bound $\frac{\Lambda}{\mu}$. The total population is never permitted to surpass it until it is below this carrying capacity by the disease-related fatalities $\delta(I+H)$. In accordance with real-world population dynamics with few resources, this mathematical feature guarantees that the model solutions stay biologically realistic, with the overall population never expanding unboundedly, since positive invariance ensures that all epidemiological trajectories starting within it will stay contained within it. Ω is the natural domain for examining the dynamics of the disease. Because it guarantees that the solutions will not diverge to implausible values, this characteristic is especially crucial for numerical simulations and long-term behavior analysis.

4.3. Existence and uniqueness

In this section, we aim to provide the verification of presence of a unique solution in the Caputo sense. By imposing Lipschitz continuity and boundedness conditions on the model equations, the well-posedness of the system is rigorously established. Thus, to maintain simplicity, we write our suggested model in the following form:

$$\begin{aligned}
&{}^{C}D^{\sigma}_{0,t}S(t) = \Xi_1(t,S),\\
&{}^{C}D^{\sigma}_{0,t}E(t) = \Xi_2(t,E),\\
&{}^{C}D^{\sigma}_{0,t}A(t) = \Xi_3(t,A),\\
&{}^{C}D^{\sigma}_{0,t}I(t) = \Xi_4(t,I),\\
&{}^{C}D^{\sigma}_{0,t}H(t) = \Xi_5(t,H),\\
&{}^{C}D^{\sigma}_{0,t}R(t) = \Xi_6(t,R)
\end{aligned} \tag{40}$$

where

$$\begin{aligned}
&\Xi_1(t,S) = \Lambda - \left(\tfrac{\beta(I+\eta A)}{N} + \mu\right) S,\\
&\Xi_2(t,E) = \tfrac{\beta(I+\eta A)}{N} S - (\varepsilon+\theta+\mu) E,\\
&\Xi_3(t,A) = \varepsilon E - (\mu+\psi+\phi+\kappa) A,\\
&\Xi_4(t,I) = \theta E + \psi A - (\mu+\delta+\omega) I,\\
&\Xi_5(t,H) = \phi A + \omega I - (\mu+\delta+\rho) H,\\
&\Xi_6(t,R) = \kappa A + \rho H - \mu R
\end{aligned} \tag{41}$$

Using the Equation (40) and the fractional-order Caputo operator,

$$\begin{aligned}
S(t) - S(0) &= \Im(\sigma)\,\Xi_1(t,S) + \Upsilon(\sigma)\int_0^t \Xi_1(\vartheta,S)\,d\vartheta,\\
E(t) - E(0) &= \Im(\sigma)\,\Xi_2(t,E) + \Upsilon(\sigma)\int_0^t \Xi_2(\vartheta,E)\,d\vartheta,\\
A(t) - A(0) &= \Im(\sigma)\,\Xi_3(t,A) + \Upsilon(\sigma)\int_0^t \Xi_3(\vartheta,A)\,d\vartheta,\\
I(t) - I(0) &= \Im(\sigma)\,\Xi_4(t,I) + \Upsilon(\sigma)\int_0^t \Xi_4(\vartheta,I)\,d\vartheta,\\
H(t) - H(0) &= \Im(\sigma)\,\Xi_5(t,H) + \Upsilon(\sigma)\int_0^t \Xi_5(\vartheta,H)\,d\vartheta,\\
R(t) - R(0) &= \Im(\sigma)\,\Xi_6(t,R) + \Upsilon(\sigma)\int_0^t \Xi_6(\vartheta,R)\,d\vartheta
\end{aligned} \tag{42}$$

where $\Upsilon(\sigma)$ and $\Im(\sigma)$ are positive real constants. We will now display the Lipchitz condition for the Caputo system (Equation 38).

Theorem 3. [76] *The vector field $\Xi_1(t,S)$, $\Xi_2(t,E)$, $\Xi_3(t,A)$, $\Xi_4(t,I)$, $\Xi_5(t,H)$ and $\Xi_6(t,R)$ fulfills the Lipchitz requirement.*

Proof: *Each component of the vector field is verified to satisfy a Lipschitz condition with respect to the state variables. For example, for the first component, it follows that*

$$\begin{aligned}
&\left\|\Xi_1(t,S) - \Xi_1\left(t,\bar{S}\right)\right\| \leq\\
&\left\|(\Lambda - (\lambda+\mu)S) - \left(\Lambda - (\lambda+\mu)\bar{S}\right)\right\|\\
&\leq (\lambda+\mu)\left\|S-\bar{S}\right\|\\
&\leq \tau_1\left\|S-\bar{S}\right\|
\end{aligned} \tag{43}$$

Assuming $\tau_1 = (\lambda+\mu)$, where λ and μ are bounded functions, similar procedures can be used to establish the norms for the remaining model equations. Then $\tau_2 = (\varepsilon+\theta+\mu)$, $\tau_3 = (\mu+\psi+\phi+\kappa)$, $\tau_4 = (\mu+\delta+\omega)$, $\tau_5 = (\mu+\delta+\rho)$, *and* $\tau_6 = \mu$

We will show that there is at least one solution to the examined Caputo model (Equation 38). Consequently, the recursive formula for (Equation 42) is as follows:

$$\begin{cases} S_n(t) = \Im(\sigma)\Xi_1 + \Upsilon(\sigma)\int_0^t \Xi_1(\vartheta, S_{n+1})\,d\vartheta, \\ E_n(t) = \Im(\sigma)\Xi_2 + \Upsilon(\sigma)\int_0^t \Xi_2(\vartheta, E_{n+1})\,d\vartheta, \\ A_n(t) = \Im(\sigma)\Xi_3 + \Psi(\sigma)\int_0^t \Xi_3(\vartheta, A_{n+1})\,d\vartheta, \\ I_n(t) = \Im(\sigma)\Xi_4 + \Phi(\sigma)\int_0^t \Xi_4(\vartheta, I_{n+1})\,d\vartheta, \\ H_n(t) = \Im(\sigma)\Xi_5 + \Phi(\sigma)\int_0^t \Xi_5(\vartheta, H_{n+1})\,d\vartheta, \\ R_n(t) = \Im(\sigma)\Xi_6 + \Phi(\sigma)\int_0^t \Xi_6(\vartheta, R_{n+1})\,d\vartheta \end{cases} \tag{44}$$

The first value of iteration are the initial conditions.

$$\begin{aligned} \Phi_{1n} &= S_n(t) - S_{n-1}(t) \\ &= \Im(\sigma)(\Xi_1(t, S_{n-1}) - \Xi_1(t, S_{n-2})) + \\ &\Upsilon(\sigma)\int_0^t (\Xi_1(\vartheta, S_{n-1}) - \Xi_1(\vartheta, S_{n-2}))d\vartheta, \end{aligned}$$

$$\begin{aligned} \Phi_{2n} &= E_n(t) - E_{n-1}(t) \\ &= \Im(\sigma)(\Xi_2(t, E_{n-1}) - \Xi_2(t, E_{n-2})) + \\ &\Upsilon(\sigma)\int_0^t (\Xi_2(\vartheta, E_{n-1}) - \Xi_1(\vartheta, E_{n-2}))d\vartheta, \\ \Phi_{3n} &= A_n(t) - A_{n-1}(t) \\ &= \Im(\sigma)(\Xi_3(t, A_{n-1}) - \Xi_3(t, A_{n-2})) + \\ &\Upsilon(\sigma)\int_0^t (\Xi_3(\vartheta, A_{n-1}) - \Xi_1(\vartheta, A_{n-2}))d\vartheta, \\ \Phi_{4n} &= I_n(t) - I_{n-1}(t) \\ &= \Im(\sigma)(\Xi_4(t, I_{n-1}) - \Xi_4(t, I_{n-2})) + \\ &\Upsilon(\sigma)\int_0^t (\Xi_4(\vartheta, I_{n-1}) - \Xi_4(\vartheta, I_{n-2}))d\vartheta, \\ \Phi_{5n} &= H_n(t) - H_{n-1}(t) \\ &= \Im(\sigma)(\Xi_5(t, H_{n-1}) - \Xi_5(t, H_{n-2})) + \\ &\Upsilon(\sigma)\int_0^t (\Xi_5(\vartheta, H_{n-1}) - \Xi_5(\vartheta, H_{n-2}))d\vartheta, \\ \Phi_{6n} &= R_n(t) - R_{n-1}(t) \\ &= \Im(\sigma)(\Xi_6(t, R_{n-1}) - \Xi_6(t, R_{n-2})) + \\ &\Upsilon(\sigma)\int_0^t (\Xi_6(\vartheta, R_{n-1}) - \Xi_6(\vartheta, R_{n-2}))d\vartheta \end{aligned}$$

It is crucial to remember that

$$\begin{aligned} &\sum_{i=0}^{n}\Phi_{1i} = S_n(t), \sum_{i=0}^{n}\Phi_{2i} = E_n(t), \sum_{i=0}^{n}\Phi_{3i} = A_n(t), \\ &\sum_{i=0}^{n}\Phi_{4i} = I_n(t), \sum_{i=0}^{n}\Phi_{5i} = H_n(t), \sum_{i=0}^{n}\Phi_{6i} = R_n(t) \end{aligned} \tag{45}$$

We analyze the following using the first equation of system (4.3).

$$\begin{aligned} \Phi_{1n} &= \|S_n(t) - S_{n-1}(t)\| \\ &= \|\Im(\sigma)(\Xi_1(t, S_{n-1}) - \Xi_1(t, S_{n-2})) + \\ &\Upsilon(\sigma)\int_0^t (\Xi_1(\vartheta, S_{n-1}) - \Xi_1(\vartheta, S_{n-2}))d\vartheta \end{aligned} \tag{46}$$

The triangle inequality is used to reduce the above equation to

$$\begin{aligned} &\|S_n(t) - S_{n-1}(t)\| \\ &\le \Im(\sigma)\|(\Xi_1(t, S_{n-1}) - \Xi_1(t, S_{n-2}))\| + \\ &\Upsilon(\sigma)\left\|\int_0^t (\Xi_1(\vartheta, S_{n-1}) - \Xi_1(\vartheta, S_{n-2}))d\vartheta\right\| \end{aligned} \tag{47}$$

Equation (43) shows that the kernel $\Xi_1(t, S)$ meets the Lipchitz condition. As a result, we can write it as follows

$$\begin{aligned} &\|S_n(t) - S_{n-1}(t)\| \le \Im(\sigma)\varpi_1\|S_{n-1} - S_{n-2}\| + \\ &\Upsilon(\sigma)\varpi_1\int_0^t \|S_{n-1} - S_{n-2}\|d\vartheta \end{aligned} \tag{48}$$

Using (45), we can simplify the above differences as follows:

$$\begin{aligned} &\|\Phi_{1n}(t)\| \le \Im(\sigma)\varpi_1\left\|\Phi_{2(n-1)}(t)\right\| + \\ &\Upsilon(\varepsilon)\varpi_1\int_0^t \left\|\Phi_{1(n-1)}(\vartheta)\right\|d\vartheta \end{aligned} \tag{49}$$

An analogous expression can also be written as under:

$$\begin{aligned}
&\|\Phi_{2n}(t)\| \leq \Im(\sigma)\varpi_2\left\|\Phi_{2(n-1)}(t)\right\| + \\
&\Upsilon(\varepsilon)\varpi_2\int_0^t\left\|\Phi_{2(n-1)}(\vartheta)\right\|d\vartheta, \\
&\|\Phi_{3n}(t)\| \leq \Im(\sigma)\varpi_3\left\|\Phi_{2(n-1)}(t)\right\| + \\
&\Upsilon(\varepsilon)\varpi_3\int_0^t\left\|\Phi_{3(n-1)}(\vartheta)\right\|d\vartheta, \\
&\|\Phi_{4n}(t)\| \leq \Im(\sigma)\varpi_4\left\|\Phi_{4(n-1)}(t)\right\| + \\
&Upsilon(\varepsilon)\varpi_4\int_0^t\left\|\Phi_{4(n-1)}(\vartheta)\right\|d\vartheta, \\
&\|\Phi_{5n}(t)\| \leq \Im(\sigma)\varpi_5\left\|\Phi_{5(n-1)}(t)\right\| + \\
&\Upsilon(\varepsilon)\varpi_5\int_0^t\left\|\Phi_{5(n-1)}(\vartheta)\right\|d\vartheta, \\
&\|\Phi_{6n}(t)\| \leq \Im(\sigma)\varpi_6\left\|\Phi_{6(n-1)}(t)\right\| + \\
&\Upsilon(\varepsilon)\varpi_6\int_0^t\left\|\Phi_{6(n-1)}(\vartheta)\right\|d\vartheta
\end{aligned} \tag{50}$$

Theorem 4. [76] *The non-integer-order system with Caputo derivative (Equation 38) possesses an analytical solution at Φ_0 if the following condition is satisfied:*

$$\Im(\sigma)\varpi_i + \Upsilon(\sigma)\varpi_i\Phi_{1,0} < 1, \quad for\, i = 1, 2, ..., 6$$

Proof: *Using equation (Equation 49) and the recursive relation, we note that the Lipschitz condition is fulfilled and compartments of model are bounded:*

$$\|\Phi_{1n}\| \leq \|S(0)\|\left[\Im(\sigma)\varpi_i + \Upsilon(\sigma)\varpi_i t\right]^n \tag{51}$$

Thus, the previously described remedies will continue to be used. However, to show that the functions mentioned above are solution of the suggested model, we obtain

$$S(t) - S(0) = S_n(t) - \varsigma_{1n}(t)$$

As a result, we have

$$\begin{aligned}
&\|\varsigma_{1n}(t)\| \leq \|\Im(\sigma)\left(\Xi_1(t, S_{n-1}) - \Xi_1(t, S_{n-2})\right) + \\
&\Upsilon(\sigma)\int_0^t\left(\Xi_1(\vartheta, S_{n-1}) - \Xi_1(\vartheta, S_{n-2})\right)d\vartheta
\end{aligned} \tag{52}$$

By applying the Lipchitz condition,

$$\begin{aligned}
&\|\varsigma_{1n}(t)\| \leq \Im(\sigma)\varpi_1\|S - S_{n-1}\| + \\
&\Upsilon(\sigma)\varpi_1\|S - S_{n-1}\|t
\end{aligned} \tag{53}$$

This offers,

$$\|\varsigma_{1n}(t)\| \leq \left(\Im(\sigma) + \Upsilon(\sigma)t\right)^{n+1}\varpi_1^{n+1}\xi \tag{54}$$

Then, at t_0, we have

$$\|\varsigma_{1n}(t)\| \leq \left(\Im(\sigma) + \Upsilon(\sigma)t_0\right)^{n+1}\varpi_1^{n+1}\xi \tag{55}$$

As n gets closer to ∞, we arrive at

$$\|\varsigma_{1n}(t)\| \to 0 \tag{56}$$

In the same direction, we can conclude for other variables. This shows that there is a solution.

Theorem 5. *It is now necessary to show that the solution obtained is single. For this, we assume that $\bar{S}(t)$ is an other solution of the studied model:*

$$\begin{aligned}
&S(t) - \bar{S}(t) = \Im(\sigma)\left(\Xi_1(t, S) - \Xi_1\left(t, \bar{S}\right)\right) + \\
&\Upsilon(\sigma)\int_0^t\left(\Xi_1(\vartheta, S) - \Xi_1\left(\vartheta, \bar{S}\right)\right)d\vartheta
\end{aligned} \tag{57}$$

Utilizing the norm on the above equation, we have:

$$\left\|S(t) - \bar{S}(t)\right\|\left(1 - \Im(\sigma)\varpi_1 + \Upsilon(\sigma)\varpi_1 t\right) \leq 0 \tag{58}$$

Theorem 6. *In the following scenario, the Caputo fractional model has a unique analytical solution*

$$\left(1 - \Im(\sigma)\varpi_1 + \Upsilon(\sigma)\varpi_1 t\right) > 0 \tag{59}$$

Proof: Note that (Equation 59) is equivalent to:

$$\left\|S(t) - \bar{S}(t)\right\|\left(1 - \Im(\sigma)\varpi_1 + \Upsilon(\sigma)\varpi_1 t\right) \leq 0 \tag{60}$$

It is therefore possible to state

$$\left\|S(t) - \bar{S}(t)\right\| = 0$$

It suggests that the result is unique and that

$$S(t) = \bar{S}(t),$$

The following results are obtained by applying the same technique to another function.

$$E = E_1, \quad A = A_1, \quad I = I_1, \quad H = H_1, \quad R = R_1 \tag{61}$$

This concludes the verification of presence of a single solution of the studied model in Caputo sense.

4.4. Hyers–Ulam–Rassias stability

The study of functional equations employs the Hyers–Ulam stability concept, which was introduced by,[103,104] which characterizes the robustness of solutions under small perturbations of their arguments. Specifically, this notion quantifies the extent to which an approximate solution remains close to an exact solution of a functional equation. Such stability properties

play a fundamental role in establishing the presence of a unique solution across multiple areas such as mathematics, physics, engineering, and economics.

In this part, we aim to prove that our suggested $SEAIHR$ COVID-19 model is Hyers–Ulam stable. For this purpose, Equation (38) is reformulated as follows:

$$\begin{aligned} &{}^{C}D_t^{\sigma}\upsilon(t) = \Xi(t,\upsilon(t)),\&\upsilon(0) = \upsilon 0,,,,, \\ &0 < t < T < \infty \end{aligned} \tag{62}$$

where $\Xi = (\Xi_1, \Xi_2, \Xi_3, \Xi_4, \Xi_5, \Xi_6)$ is a continuous vector function and $\upsilon = S, E, A, I, H, R$ is a vector.

Definition 15. *Assume that $\Xi : [0,T] \times R^6 \to R^6$ is a continuous mapping. The system (62) is Hyers–Ulam stable if the following condition holds for each solution $\sigma \in \mathbf{B}([0,T], R^6)$:*

$$\left|{}^{C}D_t^{\sigma}\upsilon - \Xi(t,\upsilon)\right| \leq N,,,,,\forall t \in [0,T]$$

there exists a solution $\upsilon \in \mathbf{B}\left([0,T], R^6\right)$ of model (62), such as

$$\left|\upsilon - \upsilon'\right| \leq \eta N,,,,,\forall t \in [0,T]$$

where $\eta > 0$ and $N > 0$.

Definition 16. *Assume that σ is the fractional order. Both $\chi : [0,T] \to R^+$ and $\Xi : [0,T] \times R^6 \to R^6$ are continuous mappings. Equation (62) possesses generalized Hyers–Ulam stability for χ if there exists $\mathbf{B}\Xi, \chi > 0$, such that the following expression holds for every solution $\upsilon \in \mathbf{B}\left([0,T], R^6\right)$*

$$\left|{}^{C}D_t^{\sigma}\upsilon(t) - \Xi(t,\upsilon(t))\right| \leq \chi(t),,,,,\forall t \in [0,T] \tag{63}$$

there exists solution $\upsilon \in \mathbf{B}\left([0,T], R^6\right)$ of Equation (62), such as

$$\left|\upsilon - \upsilon'\right| \leq \mathbf{B}_{\Xi,\chi}\chi(t),,,,,\forall t \in [0,T]$$

To prove that model (62) possesses Hyers-Ulam stability, we assume the following:

- $[\mathfrak{W}_1]\Xi : [0,T] \times R^6 \to R^6$ is a continuous mapping.
- $[\mathfrak{W}_2]\exists \mathbf{B}_{\Xi} > 0$ such that for each solution $\upsilon, \upsilon' \in \mathbf{B}\left([0,T], R^6\right)$

$$\left|\upsilon - \upsilon'\right| \leq \mathbf{B}_{\Xi}\left|\upsilon - \upsilon'\right|,,,,,\forall t \in [0,T]$$

- $[\mathfrak{W}_3]$ Let $\chi \in ([0,T], R^+)$ be an increasing mapping, and let $\mathfrak{Y}_{\chi} > 0$, such that

$$\int_0^t \chi(\vartheta)\,d\vartheta \leq \mathfrak{Y}_{\chi}\chi(t),,,,\forall \upsilon \in [0,T]$$

Theorem 7. *Assume that $[\mathfrak{W}1] - [\mathfrak{W}3]$ exist, and the generalized Equation (62) Hyers–Ulam stability with respect to χ on the interval provided that $\varphi(\sigma)\mathbf{B}\Xi < 1$.*

Proof: *Let $\upsilon' \in \mathbf{B}([0,T], \mathbb{R}^6)$ be an approximate solution of the fractional system, and let υ denote the exact solution. The system can then be written in the form*

$$\upsilon = \upsilon(0) + \varphi(\sigma)\Xi(t,\varphi) + \beth(\sigma)\int_0^t \Xi(\upsilon,\upsilon(\vartheta))\,d\vartheta$$

Subtracting the approximate solution from the exact solution gives

$$\begin{aligned} &\left|\upsilon - \upsilon(0) + \varphi(\sigma)\Xi\left(t,\varphi'\right) + \beth(\sigma)\int_0^t \Xi\left(\upsilon,\upsilon'(\vartheta)\right)d\vartheta\right| \\ &\leq \varphi(\sigma)\chi(t) + \beth(\sigma)\int_0^t \sigma(\vartheta)\,d\vartheta\& \\ &\leq \left(\varphi(\sigma) + \beth(\sigma)\mathfrak{Y}\chi\right)\chi(t). \end{aligned} \tag{64}$$

Using the Lipschitz property of the vector field Ξ, the inequality becomes

$$\begin{aligned} &\left|\upsilon - \upsilon'\right| \\ &\leq \left|\upsilon - \upsilon(0) - \varphi(\sigma)\Xi\left(t,\varphi'\right) - \beth(\sigma)\int_0^t \Xi\left(\vartheta,\upsilon'(\vartheta)\right)d\vartheta\right| \\ &\leq \left|\upsilon - \upsilon(0) - \varphi(\sigma)\Xi(t,\upsilon) - \beth(\sigma)\right. \\ &\int_0^t \Xi(\vartheta,\upsilon(\vartheta))\,d\vartheta - \varphi(\sigma)\Xi\left(t,\upsilon'\right) - \beth(\sigma)\int_0^t \Xi\left(\vartheta,\upsilon'(\vartheta)\right)d\vartheta \\ &\left.+\varphi(\sigma)\Xi\left(t,\upsilon'\right) - \beth(\sigma)\int_0^t \Xi\left(\vartheta,\upsilon'(\vartheta)\right)d\vartheta\right| \\ &\leq \left|\upsilon - \upsilon(0) - \varphi(\sigma)\Xi(t,\upsilon) - \beth(\sigma)\int_0^t \Xi(\vartheta,\upsilon(\vartheta))\,d\vartheta\right| + \\ &\varphi(\sigma)\left|\Xi(t,\upsilon) - \Xi\left(t,\upsilon'\right)\right| \\ &+\beth(\sigma)\int_0^t \left|\Xi(\vartheta,\upsilon(\vartheta)) - \Xi\left(\vartheta,\upsilon'(\vartheta)\right)\right|d\vartheta\& \leq (\varphi(\sigma) + \\ &\beth(\sigma)\mathfrak{Y}\chi\chi(t) + \\ &\varphi(\sigma)\mathfrak{W}\Xi\left|\upsilon - \upsilon'\right| + \chi(\sigma)\mathfrak{W}\Xi\int_0^t \left|\upsilon(\vartheta) - \upsilon'(\vartheta)\right|d\vartheta s \end{aligned} \tag{65}$$

Rearranging terms and assuming $\varphi(\sigma)\mathfrak{W}_{\Xi} < 1$, the inequality can be written in a form suitable for applying the fractional Gronwall inequality

$$\left|\upsilon-\upsilon'\right| \leq \frac{\left(\varphi(\sigma)+\beth(\sigma)\,\mathfrak{Y}\sigma\right)\chi(t)}{1-\varphi(\chi)\,\mathfrak{U}\beth}+\frac{\beth(\sigma)\,\mathfrak{U}\Xi}{1-\varphi(\sigma)\,\mathfrak{U}\Xi}$$
$$\int_0^t \left|\upsilon(\vartheta)-\upsilon'(\vartheta)\right|d\vartheta \tag{66}$$

Using the fractional Gronwall inequality leads to the explicit bound

$$\left|\upsilon-\upsilon'\right| \leq \left[\frac{\upsilon(\sigma)+\beth(\sigma)\,\mathfrak{Y}\chi}{1-\varphi(\sigma)\,\mathfrak{U}\Xi}\exp(t)\right]\beth(\sigma)$$

On setting $\mathfrak{U}\Xi,\chi=\left[\frac{\varphi(\sigma)+\beth(\sigma)\mathfrak{W}\chi}{1-\varphi(\sigma)\mathfrak{U}\Xi}\exp(t)\right]$, *we have*

$$\left|\upsilon-\upsilon'\right| \leq \mathfrak{U}_{\Xi,\chi}\chi(t) \tag{67}$$

where $\mathfrak{U}_{\Xi,\chi}$ *is explicitly defined in terms of the model parameters and Lipschitz constants. This inequality explicitly shows that the approximate solution* υ' *remains close to the exact solution* υ *within a bound proportional to* $\chi(t)$*, which verifies the Hyers–Ulam stability of the fractional-order system.*

4.5. Equilibrium points and reproductive number

The disease-free equilibrium, indicated by E^o and given by, is attained when there is no coronavirus in the community.

$$E^o=(S^o,E^o,A^o,I^o,H^o,R^o)=\left(\frac{\Lambda}{\mu},0,0,0,0,0\right) \tag{68}$$

For the examination of the population's COVID-19 prevalence, if the endemic equilibrium of the coronavirus model is defined as $E_*=(S^*,E^*,A^*,I^*,H^*,R^*)$, the model Equation (38) can then be simultaneously solved at steady state to provide

$$\begin{aligned}
E_* &= (S^*,E^*,A^*,I^*,H^*,R^*)\\
S^* &= \frac{\Lambda}{\lambda^*+\mu}, E^*=\frac{\lambda^*\Lambda}{\mathcal{C}_1(\lambda^*+\mu)},\\
A^* &= \frac{\varepsilon\lambda^*\Lambda}{\mathcal{C}_1\mathcal{C}_2(\lambda^*+\mu)},\\
I^* &= \frac{(\mathcal{C}_2\theta+\psi\varepsilon)\lambda^*\Lambda}{\mathcal{C}_1\mathcal{C}_2\mathcal{C}_3(\lambda^*+\mu)},\\
H^* &= \frac{[\mathcal{C}_3\phi\varepsilon+\omega(\mathcal{C}_2\theta+\psi\varepsilon)]\lambda^*\Lambda}{\mathcal{C}_1\mathcal{C}_2\mathcal{C}_3\mathcal{C}_4(\lambda^*+\mu)},\\
R^* &= \frac{[\mathcal{C}_3\mathcal{C}_4\kappa\varepsilon+\rho(\mathcal{C}_3\phi\varepsilon+\omega(\mathcal{C}_2\theta+\psi\varepsilon))]\lambda^*\Lambda}{\mathcal{C}_1\mathcal{C}_2\mathcal{C}_3\mathcal{C}_4(\lambda^*+\mu)}
\end{aligned} \tag{69}$$

where

$$\begin{aligned}
&\lambda^*=\tfrac{\beta(I^*+\eta A^*)}{N^*},\\
&C_1=(\varepsilon+\theta+\mu), \qquad C_2=(\mu+\psi+\phi+\kappa),\\
&C_3=(\mu+\delta+\omega), \qquad C_4=(\mu+\delta+\rho)
\end{aligned}$$

The basic reproduction number R_0, is a classical variable that is important to epidemiology since it governs the persistence and extinction of diseases in society. The basic reproduction number is the average number of secondary COVID-19 cases caused by a coronavirus-infected individual when they are introduced into a community that solely has susceptible individuals. The reproductive number for the studied model computed through next generation matrix technique[105] is given by:

$$R_0=\frac{\beta(\eta\varepsilon C_3+\psi\varepsilon+\theta C_2)}{C_3C_2C_1}. \tag{70}$$

The effective contact rate β, reduced infectiousness factor η, progression rates from exposed to infectious classes, and ε, θ, hospitalization, recovery parameters $\phi,\omega,\kappa,and\rho$, and disease-induced mortality δ, all of which directly affect the basic reproduction number and outbreak magnitude.

4.6. Impact of key parameters on R_0

Figure 3 presents the impact of key parameters on reproductive number R_0 through surface plots. The six subfigures show how various combinations of epidemiological parameters affect R_0, offering suggestions for possible intervention measures.

Figure 3A shows the combined influence of the lowered infectiousness parameter η and the transmission rate β on the reproductive number R_0. The surface demonstrates that R_0 rises linearly with β, suggesting that social separation and other efforts that control contact rates significantly reduce the spread of disease. η has a moderate impact on R_0. This shows the importance to find and separate acutely infected humans in order to stop the spread of COVID-19 spread. **Figure 3B** illustrates the impact of (ε) and (θ), which are the progression rates from exposed to acutely infected and exposed to infected compartments on R_0. The surface shows that R_0 is very sensitive to changes in ε, indicating that measures (such as early treatment or quarantine) that slow the transition from exposed to infectious states may be useful in preventing the spread of disease. **Figure 3C** shows the combined influence of the acutely infected progression rate ψ and the exposed progression rate ε on R_0. R_0 increases when both ψ and ε are high, highlighting the necessity of quickly identifying and isolating both acutely infected and exposed persons. The relationship between the progression rate ε and the transmission rate β is observed in **Figure 3D.** This surface plot shows that high progression rates can result in increasing R_0 values even

with low transmission rates, highlighting the significance of controlling disease progression and transmission for efficient disease management. **Figure 3E** shows the relationship between the acute infection progression rate ψ and the lowered infectiousness parameter η. The surface shows that R_0 achieves its highest values when acutely infected persons are extremely contagious and quickly move to infectious stages when ψ is high. The use of extensive testing to identify acutely infected humans is supported by this finding. **Figure 3F** shows the relationship between transmission rate β and natural death rate μ. The surface indicates that populations with greater natural turnover rates have somewhat lower R_0 values because individuals spend less time in infectious compartments, even though μ has a smaller effect than transmission parameters.

These sensitivity studies together contribute to public health decision-making by determining which parameters most strongly influence disease transmission and, thus, where intervention efforts should be focused for optimum efficacy in reducing COVID-19 outbreaks.

5. Chaos control

In this part, we stabilize the system (38) to equilibrium points using the linear feedback control method as discussed in.[106] We shall study the fractional-order system in its controlled form Equation (38) as follows:

$$\begin{aligned}
&{}^{C}D_t^{\sigma} S(t) = \Lambda - (\lambda+\mu) S + a_1 (S - S^{\circ}),\\
&{}^{C}D_t^{\sigma} E(t) = \lambda S - (\varepsilon+\theta+\mu) E + a_2 (E - E^{\circ}),\\
&{}^{C}D_t^{\sigma} A(t) = \varepsilon E - (\mu+\psi+\phi+\kappa) A + a_3 (A - A^{\circ}),\\
&{}^{C}D_t^{\sigma} I(t) = \theta E + \psi A - (\mu+\delta+\omega) I + a_4 (I - I^{\circ}),\\
&{}^{C}D_t^{\sigma} H(t) = \phi A + \omega I - (\mu+\delta+\rho) H + a_5 (H - H^{\circ}),\\
&{}^{C}D_t^{\sigma} R(t) = \kappa A + \rho H - \mu R + a_6 (R - R^{\circ}).
\end{aligned} \tag{71}$$

where $a_i, i = 1, 2, \cdots 6$ are control variables representing practical intervention strategies and E° (Equation 38) denotes the COVID - free equilibrium points

For the Equation (71), the Jacobian matrix at COVID-free equilibrium points E° takes the form as:

$$J(E^{\circ}) = \begin{bmatrix}
-a_1-\mu & 0 & -\frac{\Lambda\beta\eta}{\mu N} & -\frac{\Lambda}{\mu}\beta & 0 & 0\\
0 & -a_2-\epsilon-\mu-\theta & \frac{\Lambda\beta\eta}{\mu N} & \frac{\Lambda}{\mu}\beta & 0 & 0\\
0 & \epsilon & -a_3-\kappa-\mu-\phi-\psi & 0 & 0 & 0\\
0 & \theta & \psi & -a_4-\delta-\mu-\omega & 0 & 0\\
0 & 0 & \phi & \omega & -a_5-\delta-\mu-\rho & 0\\
0 & 0 & \kappa & 0 & \rho & -a_6-\mu
\end{bmatrix}$$

Using the control variables $a_1 = 1, a_2 = 2, a_3 = 3, a_4 = 4, a_5 = 5, a_6 = 6$ and the parameter values listed in Table 1, and employing the COVID-free equilibrium points, the characteristic equation from the above Jacobian matrix is obtained as follows:

$$\begin{aligned}
C(\lambda) = {} & \lambda^6 - 240760\lambda^5 - 106460\lambda^4 - 18130\lambda^3 -\\
& 966.4878\lambda^2 + 21.7938\lambda - 152430
\end{aligned} \tag{72}$$

In addition, the roots of Equation (72) are as $\lambda_1 = -1.0128$, $\lambda_2 = -6.0128$, $\lambda_3 = -5.1448$, $\lambda_4 = -31.3050$, $\lambda_5 = -36.6927$, and $\lambda_6 = -4.2358$. Thus, COVID-free equilibrium points E° are stable since all eigenvalues are negative.

Since the system is of fractional order $0 < \sigma < 1$, the Matignon stability criterion can be applied, which states that a fractional-order linear system is asymptotically stable if all eigenvalues satisfy

$$|\arg(\lambda_i)| > \frac{\sigma\pi}{2}, \quad i = 1, 2, \ldots, 6$$

All eigenvalues λ_i are real and negative, hence $\arg(\lambda_i) = \pi$. Therefore, for any $0 < \sigma < 1$, we have:

$$\pi > \frac{\sigma\pi}{2}.$$

This confirms that the Matignon criterion is satisfied. Consequently, the COVID-free equilibrium points E° are asymptotically stable for the fractional-order system under the chosen control strategy.

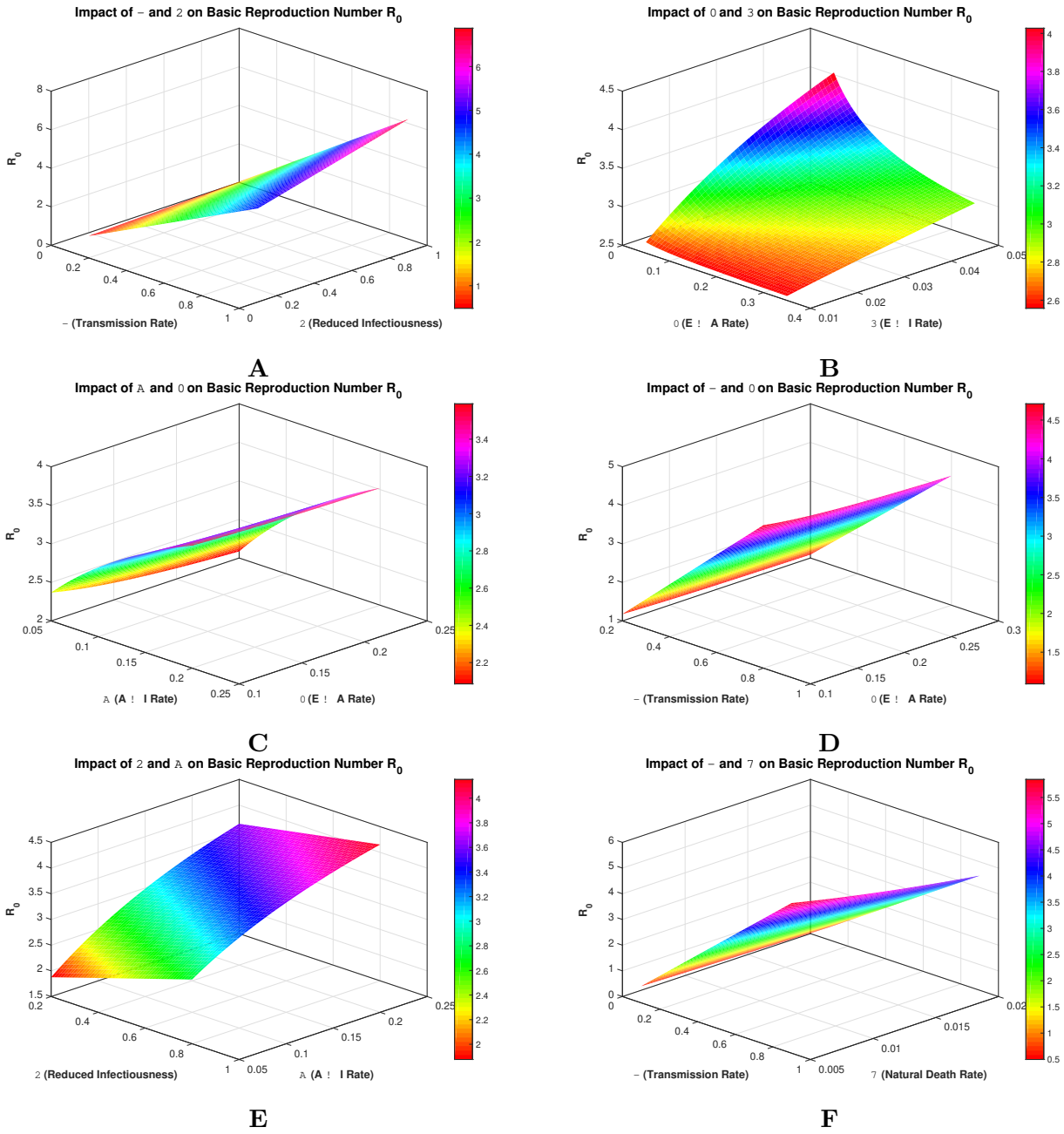

Figure 3. Impact of parameters on reproduction number R_0 through surface plots. (A) Influence of transmission rate and reduced infectiousness on reproductive number. (B) Influence of progression rates and θ on reproductive number. (C) Influence of acutely infection progression and ε on reproductive number. (D) Combined impact of β and ε on reproductive number. (E) Relation between η and ψ on reproductive number. (F) Impact of β and natural death rate μ on reproductive number.

6. Numerical scheme

The Caputo fractional derivative is approximated using Newton polynomials[107] in the suggested numerical approach, which has a number of benefits over traditional techniques. When compared to conventional methods, it offers better accuracy and higher-order convergence rates, especially for non-smooth solutions. Physical characteristics like improved stability of the fractional model system are preserved by an unconditionally stable structure. By lowering memory requirements through polynomial interpolation of historical data, it offers computational efficiency. It may be readily extended to higher dimensions and adjusted to different mesh structures. It is accurate over a large range of fractional orders.

To keep things simple, we can describe the Equation (38) as follows:

$$\begin{aligned}
{}^{C}D_{t}^{\sigma}S\left(t\right) &= \Xi_{1}\left(t,S\right),\\
{}^{C}D_{t}^{\sigma}E\left(t\right) &= \Xi_{2}\left(t,E\right),\\
{}^{C}D_{t}^{\sigma}A\left(t\right) &= \Xi_{3}\left(t,A\right),\\
{}^{C}D_{t}^{\sigma}I\left(t\right) &= \Xi_{4}\left(t,I\right),\\
{}^{C}D_{t}^{\sigma}H\left(t\right) &= \Xi_{5}\left(t,H\right),\\
{}^{C}D_{t}^{\varepsilon}R\left(t\right) &= \Xi_{6}\left(t,R\right)
\end{aligned} \tag{73}$$

So,

$$S\left(t\right)-S\left(0\right)=\frac{1-\sigma}{\Gamma\left(\sigma\right)}\int_{0}^{t}\Xi_{1}\left(\vartheta,S\left(\vartheta\right)\right)\left(t-\vartheta\right)^{\sigma-1}d\vartheta \tag{74}$$

We can write as follows at the moment $t_{a+1}=(a+1)\Delta t$:

$$S\left(t_{a+1}\right)-S\left(0\right)=\frac{1-\sigma}{\Gamma\left(\sigma\right)}\int_{0}^{t_{i+1}}\Xi_{1}\left(\vartheta,S\left(\vartheta\right)\right)\left(t_{a+1}-\vartheta\right)^{\sigma-1}d\vartheta \tag{75}$$

As a result,

$$S\left(t_{a+1}\right)=S\left(0\right)+\frac{1-\sigma}{\Gamma\left(\sigma\right)}\sum_{c=2}^{a}\int_{t_{c}}^{t_{c+1}}\Xi_{1}\left(\vartheta,S\left(\vartheta\right)\right)\left(t_{a+1}-\vartheta\right)^{\sigma-1}d\vartheta \tag{76}$$

The Newton polynomial can be replaced by Equation (76) to produce

$$\begin{aligned}
S^{a+1}=S_{0}+\frac{1-\sigma}{\Gamma\left(\sigma\right)}\sum_{c=2}^{a}\int_{t_{c}}^{t_{c+1}}\Bigg\{&\Xi_{1}\left(t_{c-2},S^{c-2}\right)+\frac{\Xi_{1}\left(t_{c-1},S^{c-1}\right)-\Xi_{1}\left(t_{c-2},S^{c-2}\right)}{\Delta t}\left(\vartheta-t_{c-2}\right)\\
&\frac{\Xi_{1}\left(t_{c},S^{c}\right)-2\Xi_{1}\left(t_{c-1},S^{c-1}\right)-\Xi_{1}\left(t_{c-2},S^{c-2}\right)}{2\left(\Delta t\right)^{2}}\left(\vartheta-t_{c-2}\right)\left(\vartheta-t_{c-1}\right)\Bigg\}\times\left(t_{a+1}-\sigma\right)^{\sigma-1}d\vartheta
\end{aligned} \tag{77}$$

As a result, the preceding equation can be rewritten as follows:

$$\begin{aligned}
S^{a+1}=S_{0}+\frac{1-\sigma}{\Gamma\left(\sigma\right)}\sum_{c=2}^{a}\Bigg\{&\int_{t_{c}}^{t_{c+1}}\Xi_{1}\left(t_{c-2},S^{c-2}\right)\left(t_{i+1}-\vartheta\right)^{\sigma-1}d\vartheta\\
&+\int_{t_{c}}^{t_{c+1}}\frac{\Xi_{1}\left(t_{c-1},S^{c-1}\right)-\Xi_{1}\left(t_{c-2},S^{c-2}\right)}{\Delta t}\left(\vartheta-t_{c-2}\right)\left(t_{a+1}-\vartheta\right)^{\sigma-1}d\vartheta\\
&+\int_{t_{c}}^{t_{c+1}}\frac{\Xi_{1}\left(t_{c},S^{c}\right)-2\Xi_{1}\left(t_{c-1},S^{c-1}\right)-\Xi_{1}\left(t_{c-2},S^{c-2}\right)}{2\left(\Delta t\right)^{2}}\left(\vartheta-t_{c-2}\right)\left(\vartheta-t_{c-1}\right)\left(t_{a+1}-\sigma\right)^{\sigma-1}d\vartheta\Bigg\}.
\end{aligned} \tag{78}$$

Consequently,

$$S^{a+1} = S_0 + \frac{1-\sigma}{\Gamma(\sigma)} \sum_{c=2}^{a} \Xi_1\left(t_{c-2}, S^{c-2}\right) \int_{t_c}^{t_{c+1}} (t_{a+1} - \vartheta)^{\sigma-1} d\vartheta$$
$$+ \frac{1}{\Gamma(\sigma)} \sum_{c=2}^{a} \frac{\Xi_1\left(t_{c-1}, S^{c-1}\right) - \Xi_1\left(t_{c-2}, S^{c-2}\right)}{\Delta t} \int_{t_c}^{t_{c+1}} (\vartheta - t_{c-2})(t_{a+1} - \vartheta)^{\sigma-1} d\vartheta$$
$$+ \frac{1}{\Gamma(\sigma)} \sum_{c=2}^{a} \frac{\Xi_1(t_c, S^c) - 2\Xi_1\left(t_{c-1}, S^{c-1}\right) - \Xi_1\left(t_{c-2}, S^{c-2}\right)}{2(\Delta t)^2} \int_{t_c}^{t_{c+1}} (\vartheta - t_{c-2})(\vartheta - t_{c-1})(t_{a+1} - \sigma)^{\sigma-1} d\vartheta \tag{79}$$

Equation (79) allows us to compute the previously mentioned integrals

$$\int_{t_c}^{t_{c+1}} (t_{a+1} - \vartheta)^{\sigma-1} d\vartheta = \frac{(\Delta t)^\sigma}{\sigma} \left[(a-c+1)^\sigma - (a-c)^\sigma\right],$$

$$\int_{t_c}^{t_{c+1}} (\vartheta - t_{c-2})(t_{a+1} - \vartheta)^{\sigma-1} d\vartheta = \frac{(\Delta t)^{\sigma+1}}{\sigma(\sigma+1)} \left[(a-c+1)^\sigma (a-c+3+2\sigma) - (a-c)^\sigma (a-c+3+3\sigma)\right],$$

$$\int_{t_c}^{t_{c+1}} (\vartheta - t_{c-2})(\vartheta - t_{c-1})(t_{a+1} - \sigma)^{\sigma-1} d\vartheta = \frac{(\Delta t)^{\sigma+2}}{\sigma(\sigma+1)(\sigma+2)}$$
$$\times \left[\begin{array}{l} (a-c+1)^\sigma \left[\begin{array}{l} 2(a-c)^2 + (3\sigma+10)(a-c) \\ +2\sigma^2 + 9\sigma + 12 \end{array} \right] \\ -(a-c)^\sigma \left[\begin{array}{l} 2(a-c)^2 + (5\sigma+10)(a-c) \\ +6\sigma^2 + 18\sigma + 12 \end{array} \right] \end{array} \right]$$

We may see the following approach if we insert the values into Equation (79).

$$S^{a+1} = S_0 + \frac{(\Delta t)^\sigma}{\Gamma(\sigma+1)} \sum_{c=2}^{a} \Xi_1\left(t_{c-2}, S^{c-2}\right) \times \Theta$$
$$+ \frac{(\Delta t)^\sigma}{\Gamma(\sigma+2)} \sum_{c=2}^{a} \left[\Xi_1\left(t_{c-1}, S^{c-1}\right) - \Xi_1\left(t_{c-2}, S^{c-2}\right)\right] \times \Theta_1 \tag{80}$$
$$+ \frac{(\Delta t)^{\sigma+2}}{\sigma(\sigma+1)(\sigma+2)} \sum_{c=2}^{a} \left[\Xi_1(t_c, S^c) - 2\Xi_1\left(t_{c-1}, S^{c-1}\right) - \Xi_1\left(t_{c-2}, S^{c-2}\right)\right] \times \Theta_2$$

Similarly, we may write from the system's other Equations (7).
Here,

$$\Theta = \left[(a-c+1)^\sigma - (a-c)^\sigma\right],$$
$$\Theta_1 = \left[(a-c+1)^\sigma (a-c+3+2\sigma) - (a-c)^\sigma (a-c+3+3\sigma)\right],$$
$$\Theta_2 = \left[\begin{array}{l} (a-c+1)^\sigma \left[\begin{array}{l} 2(a-c)^2 + (3\sigma+10)(a-c) \\ +2\sigma^2 + 9\sigma + 12 \end{array} \right] \\ -(a-c)^\sigma \left[\begin{array}{l} 2(a-c)^2 + (5\sigma+10)(a-c) \\ +6\sigma^2 + 18\sigma + 12 \end{array} \right] \end{array} \right]$$

Remark: The Newton polynomial based scheme developed for the Caputo fractional order system ensures consistency with the integral formulation of the fractional derivative and accurately approximates the memory-dependent terms. The method satisfies convergence under standard Lipschitz conditions and maintains numerical stability for different fractional orders. Additionally, it preserves essential qualitative properties of the model, including positivity and boundedness of solutions. These properties confirm that the scheme is both mathematically reliable and biologically consistent for long-term COVID-19 simulations.

7. Numerical simulation of the proposed scheme

The graphs illustrate the dynamic behavior of the six epidemiological compartments susceptible S(t), exposed E(t), acutely infected A(t), infectious I(t), hospitalized H(t), and recovered R(t) when the COVID-19 model is formulated using the fractional Caputo operator. The fractional order σ controls the memory effect of the system, where smaller values of σ introduces stronger memory and nonlocal behavior into the disease transmission process. The primary motivation for employing fractional derivatives is their ability to capture long-term dependence and non-exponential decay behavior through the fractional parameter σ, thereby enhancing model flexibility and realism. This framework allows more accurate representation of complex epidemic patterns and provides improved agreement with observed data compared to classical integer-order approaches. The **Figure (4)** shows a decreasing trend as individuals leave the susceptible population through infection. As the fractional order decreases, the decline in S(t) becomes gradually slower. This indicates that stronger memory effects reduce the effective transmission rate, causing susceptible individuals to remain in their class for longer durations. The exposed population in **Figure (5)** displays very slight variations over time, with higher values observed at larger fractional orders. When σ decreases, E(t) becomes smaller, reflecting that with stronger memory effects, the transition from susceptible to exposed is moderated. This leads to reduced accumulation of newly exposed individuals. The acutely infected class in **Figure (6)** remains nearly constant, with minimal fluctuations as time evolves. Higher fractional orders produce slightly larger values of A(t). The results demonstrate that fractional dynamics suppress sharp transitions, stabilizing the acute infection level and preventing rapid escalation. The **Figure (6)** shows that the infectious population increases gently with time. Lower fractional orders lead to noticeably reduced values of I(t), indicating that memory-driven fractional dynamics delay and weaken the progression from acute to infectious stages. This effect highlights the role of fractional operators in slowing disease propagation. Similar to **Figure (7)**, the hospitalized class in **Figure (8)** also experiences a mild rise over time. As σ decreases, H(t) becomes lower, implying that fractional memory reduces the flow of infected individuals into hospitalization. This behavior reflects a more diffuse, delayed progression through the disease stages. The recovered class in **Figure (9)** shows a smooth upward trend. Larger fractional orders yield higher recovery values, whereas decreasing σ slows the accumulation of recovered individuals. This confirms that fractional dynamics slow down the recovery process, consistent with the delayed transitions observed in other compartments. These results demonstrate the flexibility and realism of fractional-order modeling, particularly its ability to account for historical effects, latency, behavioral response delay, and other nonlocal influences inherent in real-world disease dynamics. The results show that decreasing σ leads to slower decay of infected and hospitalized populations, indicating stronger memory effects and prolonged disease persistence. Biologically, this reflects delayed immune response and extended infectious periods, confirming that fractional dynamics capture non-exponential transmission patterns more realistically than classical models. Variations in key epidemiological parameters significantly influence the outbreak dynamics of the SEAIHR fractional model. Changes in the transmission rate β, progression rates ε, θ, and hospitalization-related parameters directly modify the peak magnitude and timing of infected and hospitalized populations, while recovery κ, and ρ and mortality δ rates strongly affect the reduction of active cases and long-term stability. The fractional order σ plays a crucial role in controlling memory intensity, where lower values lead to slower decay and prolonged infection persistence. Unlike classical integer-order models, the Caputo fractional operator incorporates past disease history into current dynamics, resulting in more flexible epidemic trajectories, improved data fitting, and a more realistic representation of delayed biological responses.

7.1. Phase plots analysis

Figure 10A shows the connection between susceptible and exposed populations over time. Biologically, this graph shows how the disease transmission influences the change from susceptibility to exposure. High infection rates decrease the susceptible humans initially, followed by a slow stabilization as the system tends to the equilibrium position. Given the rapid starting drop, this trajectory illustrates the significance of early intervention steps to flatten the curve from a policy point of view. The convergence toward equilibrium implies that in the absence of continuous control efforts, the disease forms an endemic state in which a particular class of

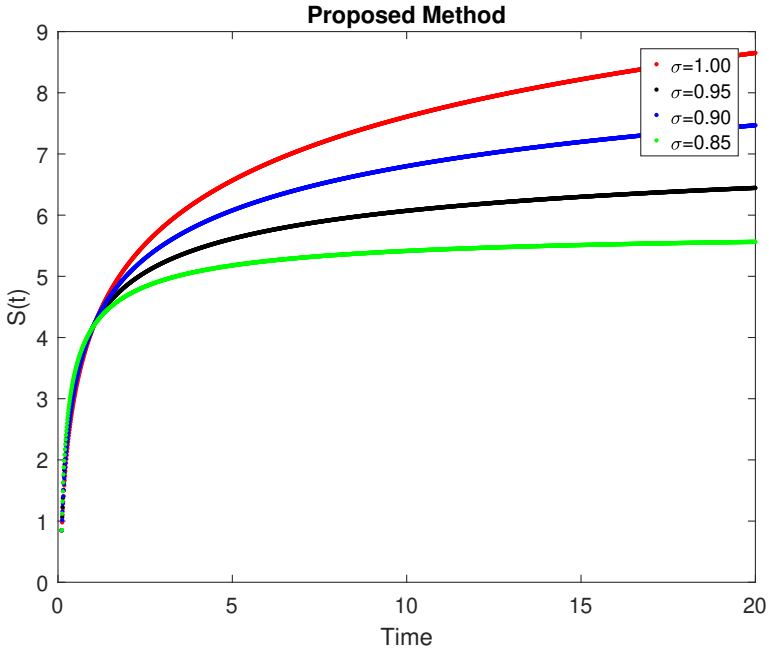

Figure 4. Simulation of S at different fractional order

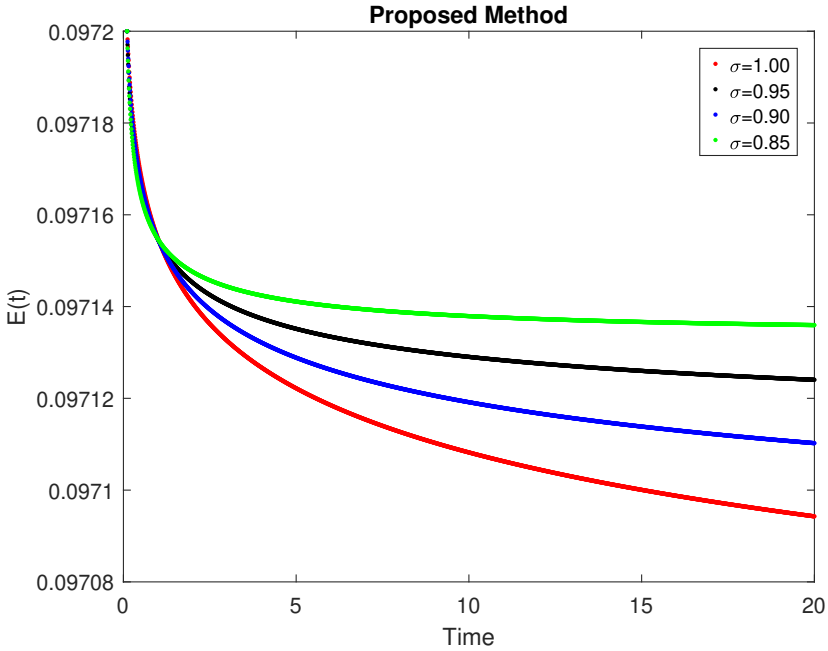

Figure 5. Simulation of E at different fractional order

the population moves toward the susceptible class while others become exposed due to persistent transmission. **Figure 10B** shows the relation between asymptomatic and infected humans. This graph is biologically relevant because it depicts the infection progression from asymptomatic to infected stages, which is essential for comprehending disease dynamics and allocating healthcare resources. The curve highlights the difficulty of managing diseases with significant asymptomatic transmission by demonstrating how asymptomatic cases can build up before appearance of infected cases. The policy implications from the plot highlight the importance of complete testing methods that identify asymptomatic carriers since their presence greatly affects the spread of the disease and makes disease eradication more difficult. The important connection between hospitalized and infected humans is observed in **Figure 10C**. Biologically, this connection shows the strain that disease epidemics place on healthcare

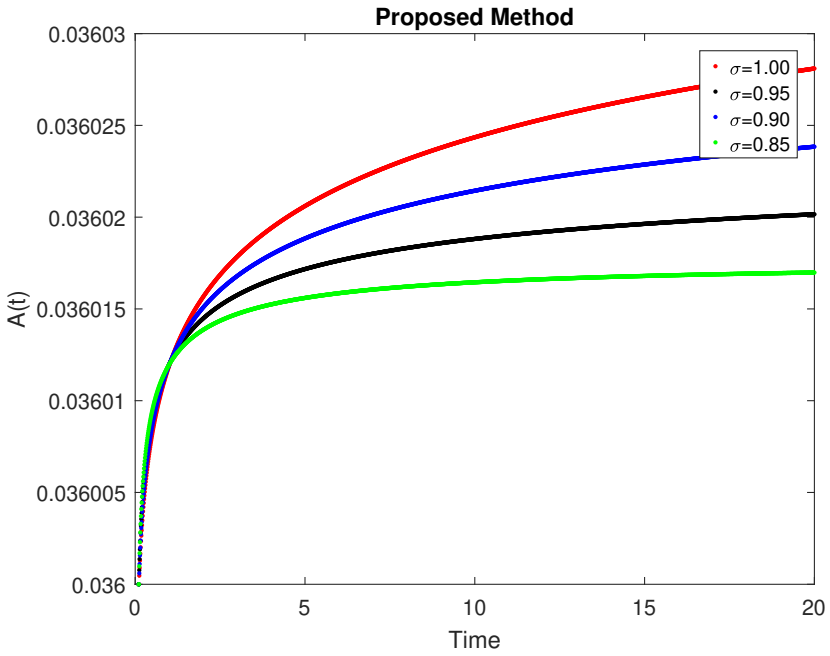

Figure 6. Simulation of A at different fractional order

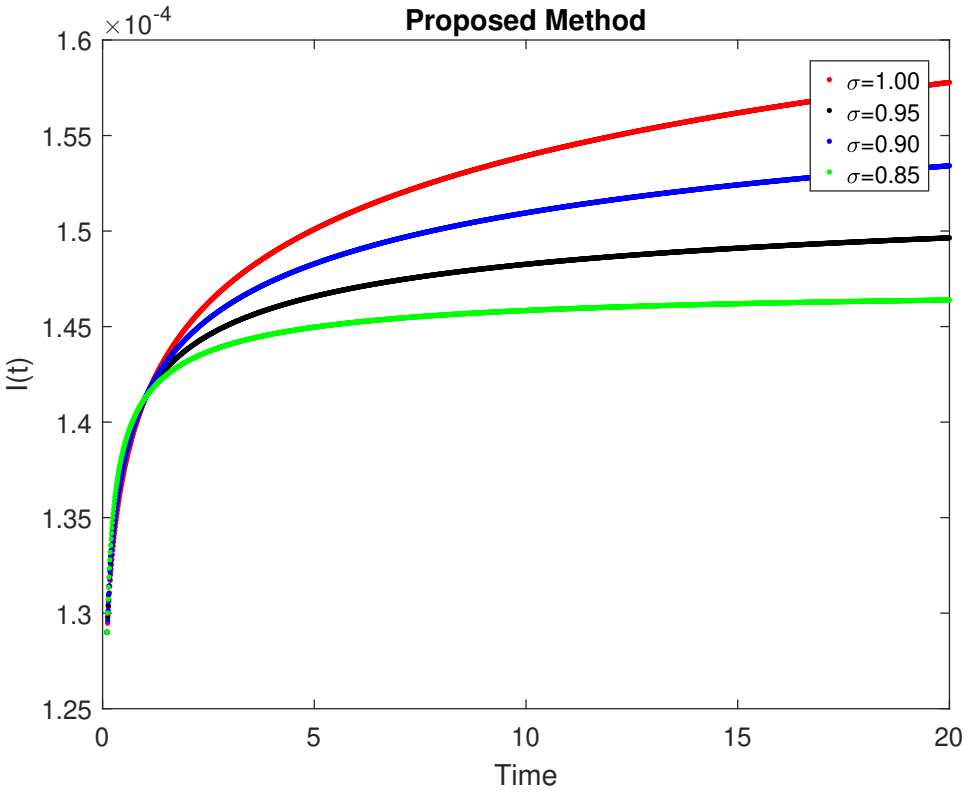

Figure 7. Simulation of I at different fractional order

systems. The plot illustrates how infected people move into hospitalized states, and the rate at which this happens affects both disease mortality and the burden on the healthcare system. From a policy point of view, this plot signifies how important it is to maintain a sufficient number of hospital beds and put policies in place to lower the hospitalization rate, like early treatment guidelines and focused interventions for high-risk groups. The curve shows that hospitalization rates may fluctuate nonlinearly with infection prevalence, indicating possible threshold effects in healthcare system overload. **Figure 10D** shows the relationship

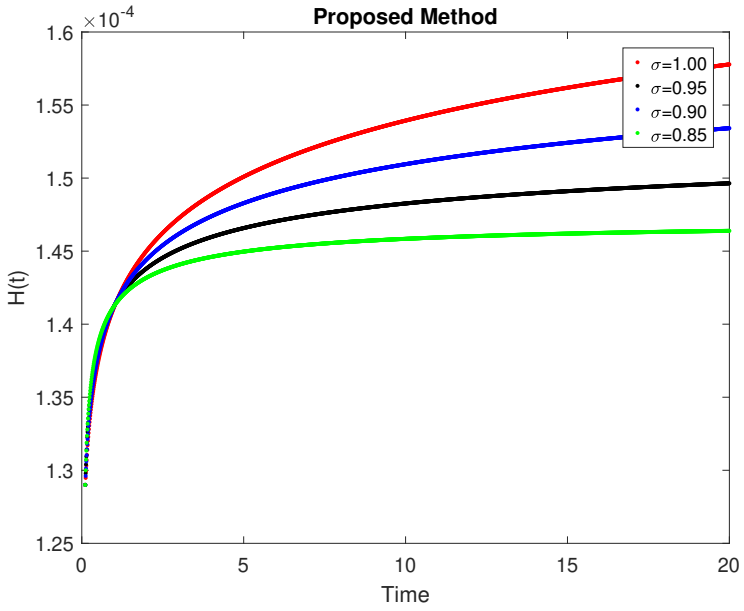

Figure 8. Simulation of H at different fractional order

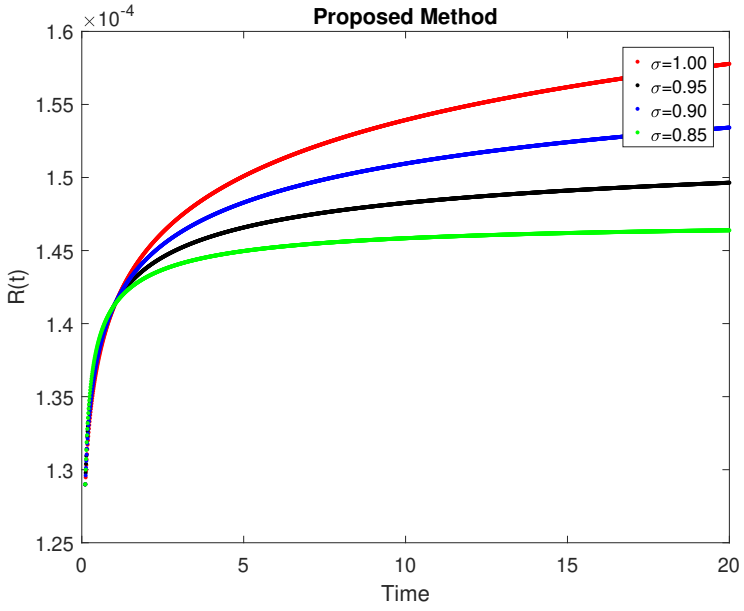

Figure 9. Simulation of R at different fractional order

between hospitalized and recovered people, which illustrates the recovery dynamics and the efficiency of the healthcare system. Biologically, this figure illustrates the recovery process and the effects of treatment as infected humans move from sickness to recovery. Hospitalization and recovery are positively correlated, suggesting that successful patient outcomes are influenced by quality medical care. For the success of the healthcare system, this discussion recommends that strengthening healthcare infrastructure, guaranteeing appropriate treatment procedures, and tracking recovery rates should be adopted. The curve reflects that better hospital treatment might greatly boost recovery rates, lower disease mortality, and shorten illness duration.

Figure 10E offers a comprehensive understanding of early infection dynamics by providing a combined relationship between susceptible, exposed, and acutely infected humans. This graph is biologically significant as it interconnects various compartments and the multi-stage nature of illness progression. The three-dimensional plot illustrates the complex feedback processes involved in the spread of disease by showing how variation in one compartment impacts the others. This illustration highlights the necessity of

intervention techniques that address several phases of infection from a policy standpoint. The trajectory highlights the significance of combined public health measures addressing all facets of disease transmission and development by indicating that interventions concentrating on any one compartment may have cascade impacts on the entire system. **Figure 10F** shows the relationship between hospitalization, recovery, and infected humans. Biologically, this graph depicts the entire duration of the COVID-19 disease, from active infection to medical intervention to final healing. The three dimensions of this plot highlight the connections between various disease outcomes and the ways in which interventions in one area might impact outcomes in others. The significance of combined healthcare approaches that address the continuum of treatment from infection detection through hospitalization to post-recovery follow-up is one of the policy implications gained from this investigation. According to the trajectory, improving the transition between these states by prompt interventions can greatly enhance overall illness outcomes and lessen the epidemic's long-term effects on population health.

8. Conclusion

This study has presented a detailed and systematic examination of fractional-order mathematical models developed to study the transmission dynamics of COVID-19. By surveying a wide range of fractional and fractal-fractional operators, including Caputo, Caputo–Fabrizio, Atangana-Baleanu, and FFM-based formulations, the study demonstrates how memory effects, hereditary properties, and nonlocal interactions significantly enhance the realism of epidemic modeling. Theoretical analyses such as positivity, boundedness, equilibrium behavior, reproduction number assessment, existence and uniqueness of solutions, Hyers–Ulam–Rassias stability, and chaos control confirm the mathematical robustness of these models. The proposed numerical scheme offers improved accuracy and stability in solving the fractional-order model compared to existing schemes. By efficiently handling memory effects and nonlinear dynamics, it provides reliable predictions of infection and hospitalization trends, making it a robust tool for analyzing epidemic scenarios and assessing control strategies. The significance of these findings lies in the clear superiority of fractional-order frameworks over classical integer-order models, as they provide substantially better fits to real-world COVID-19 data by naturally incorporating long term memory and anomalous diffusion behaviors that are inherent to infectious disease spread. This enhanced realism translates into more reliable predictions of epidemic trajectories, enabling more effective evaluation of control interventions such as vaccination, quarantine, and environmental mitigation strategies, ultimately supporting policymakers in reducing infections, hospitalizations, and mortality on a global scale. Overall, fractional-order COVID-19 models represent a powerful and reliable modeling paradigm for understanding complex infectious disease dynamics. Future research may focus on data-driven parameter estimation, stochastic fractional models, and hybrid machine-learning fractional approaches to further improve prediction accuracy and decision-making in public health policy.

Acknowledgments

The authors extend their appreciation to Prince Sattam bin Abdulaziz University for funding this research work through the project number (PSAU/2025/RV/12).

Funding

This work is funded by Prince Sattam bin Abdulaziz University, project number (PSAU/2025/RV/12).

Conflict of interest

The authors declare they have no competing interests.

Author contributions

Conceptualization: Kottakkaran Sooppy Nisar, Muhammad Farman
Formal analysis: Muhammad Kamran, Muhammad Farman
Investigation: Kottakkaran Sooppy Nisar, Muhammad Farman, Muhammad Kamran
Methodology: Kottakkaran Sooppy Nisar, Muhammad Farman, Khadija Jamil
Writing–original draft: Muhammad Farman, Khadija Jamil
Writing–review & editing: Kottakkaran Sooppy Nisar, Muhammad Kamran, Muhammad Farman

Availability of data

Not applicable.

AI tools statement

All authors confirm that no AI tools were used in the preparation of this manuscript.

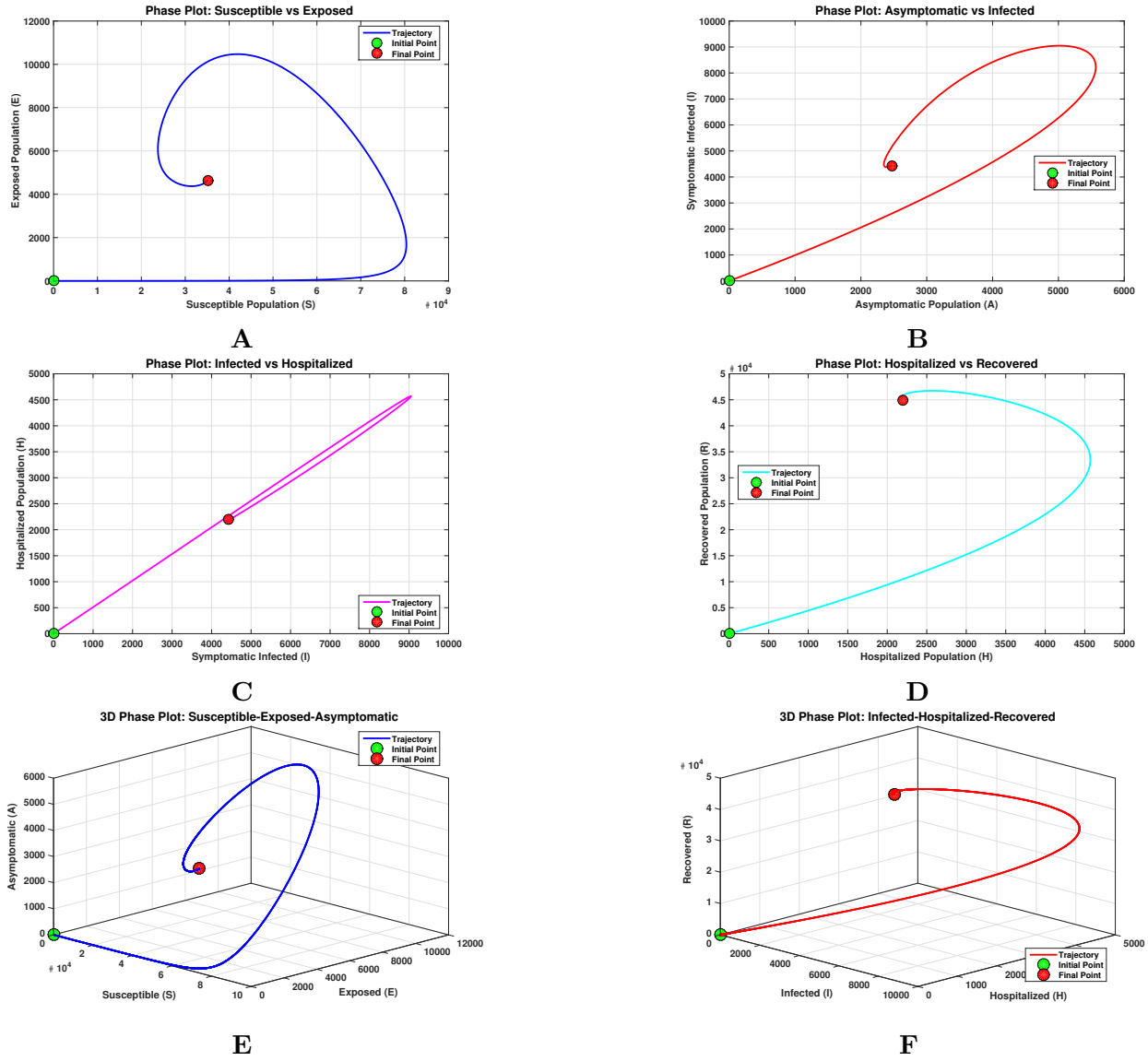

Figure 10. Phase plots showing the relationship between different compartments of the model. (A) Susceptible versus exposed humans plot. The curve starts at the initial condition denoted by the green circle and converges to the red circle, which represents the endemic equilibrium point. The dynamic interaction between the susceptible and exposed compartments is shown by the curve, which also shows how the force of infection moves people from the susceptible class to the exposed class. (B) Phase plot showing the relationship of asymptomatic and infected humans. The curve shows how COVID progresses from an asymptomatic human to an infected human, and the slope shows how frequently these changes occur. Within the infected class, the balance between natural disease progression and recovery process is shown by the initial conditions and final equilibrium. (C) Phase diagram comparing hospitalized and infected humans. The figure shows how people move from infection to hospitalized states; the hospitalization rate and capacity limitations of the healthcare system are reflected in the curvature of the plot. Planning for healthcare resources and intervention techniques are directly impacted by the relationships between these divisions. (D) Phase plot showing relationship between hospitalized and recovered humans. This illustration shows the efficacy of both natural recovery process and medical treatment by following the recovery pathway from hospitalization to complete recovery. The increasing curve illustrates both the rate of recovery and the importance of medical care given to hospitalized patients. (E) Three-dimensional phase plot illustration of acutely infected, exposed, and vulnerable humans. This comprehensive depiction shows the complex dynamics of infection transmission along several paths by capturing the interactions among the initial illness states. The progressive process from vulnerability through exposure to acutely infected class is shown by the helical trajectory. (F) Three-dimensional phase plot showing the relationship between hospitalized, recovered, and infected humans. This diagram captures the entire range of disease outcomes by showing the entire process from active infection through hospitalization to recovery. The complex trajectory shows how the severity of the illness, the use of healthcare, and the healing process are all interconnected.

References

1. Algehyne EA, Din R ud. On global dynamics of COVID-19 by using SQIR type model under non-linear saturated incidence rate. *Alex Eng J.* 2021;60(1):393-399. https://doi:10.1016/j.aej.2020.08.040
2. Aljadeed R, AlRuthia Y, Balkhi B, et al. The Impact of COVID-19 on Essential Medicines and Personal Protective Equipment Availability and Prices in Saudi Arabia. *Healthcare.* 2021;9(3):290. https://doi.org/10.3390/healthcare9030290
3. World Health Organization. WHO Coronavirus (COVID-19) Dashboard. World Health Organization. Updated March 14, 2026. Accessed March 14, 2026. https://covid19.who.int/
4. Jiang XL, Qiu Y, Zhang YP, et al. Zhonghua Yu Fang Yi Xue Za Zhi [Latent period and incubation period with associated factors of COVID-19 caused by Omicron variant]. *Chin J Prev Med.* 2023;57(5):659-666. https://doi.org/10.3760/cma.j.cn112150-20220926-00925
5. Inaba S, Nakao Y, Ikeda S, et al. Simple Symptom-Based Prediction of COVID-19: A Single-Center study of outpatient fever clinic in Japan. *Cureus.* 2023;15(3):e36614. https://doi.org/10.7759/cureus.36614
6. Karmaker CL, Ahmed T, Ahmed S, Ali SM, Moktadir MdA, Kabir G. Improving supply chain sustainability in the context of COVID-19 pandemic in an emerging economy: Exploring drivers using an integrated model. *Sustainable Production and Consumption.* 2021;26:411-427. https://doi.org/10.1016/j.spc.2020.09.019
7. Deng L, Lee C, Lee S, Ding Y, Song Y, Newman G. Mental health among U.S. College students: implications of COVID-19 and roles of institutional and individual characteristics. *J Am Coll Health.* 2024;73(4):1640-1651. https://doi.org/10.1080/07448481.2024.2346349
8. Kermack WO, McKendrick AG. A contribution to the mathematical theory of epidemics. *Proceedings of the Royal Society of London Series A, Containing Papers of a Mathematical and Physical Character.* 1927;115(772):700-721. https://doi.org/10.1098/rspa.1927.0118
9. Mekonen, K. G., Aragaw, F. M., Aknda, K. T. Optimal control analysis on the impact of non-pharmaceutical interventions and vaccination on the dynamics of COVID-19. Results in Control and Optimization. 2023;13:100319. https://doi.org/10.1016/j.rico.2023.100319
10. Yang B, Yu Z, Cai Y. The impact of vaccination on the spread of COVID-19: Studying by a mathematical model. *Physica A: Statistical Mechanics and its Applications.* 2021;590:126717. https://doi.org/10.1016/j.physa.2021.126717
11. Huang B, Wang J, Cai J, et al. Integrated vaccination and physical distancing interventions to prevent future COVID-19 waves in Chinese cities. *Nat Hum Behav.* 2021;5(6):695-705. https://doi.org/10.1038/s41562-021-01063-2
12. Ferguson N, Laydon D, Nedjati-Gilani G, Imai N, Ainslie K, Baguelin M, et al. Impact of non-pharmaceutical interventions (NPIs) to reduce COVID- 19 mortality and healthcare demand. *Imperial College London.* 2020;16. https://doi.org/10.25561/77482
13. Naik PA, Yeolekar BM, Qureshi S, Yeolekar M, Madzvamuse A. Modeling and analysis of the fractional-order epidemic model to investigate mutual influence in HIV/HCV co-infection. *Nonlinear Dyn.* 2024;112(13):11679-11710. https://doi.org/10.1007/s11071-024-09653-1
14. Khan MA, Ozdemir N, Ahmad I, Isa NM, Alzahrani E. Modeling and analysis of HIV/AIDS spread in Pakistan: Role of optimal control and behavioral changes. *J Comput Appl Math.* 2026;473:116913. https://doi.org/10.1016/j.cam.2025.116913
15. Jamil S, Farman M, Akgül A. Qualitative and quantitative analysis of a fractal fractional HIV/AIDS model. *Alex Eng J.* 2023;76:167-177. https://doi.org/10.1016/j.aej.2023.06.021
16. Uçar E. Tuberculosis disease dynamics with fractal-fractional derivative under the use of real data. *J Comput Appl Math.* 2025;473:116889. https://doi.org/10.1016/j.cam.2025.116889
17. Uçar S. Analysis of hepatitis B disease with fractal fractional Caputo derivative using real data from Turkey. *J Comput Appl Math.* 2023;419:114692. https://doi.org/10.1016/j.cam.2022.114692
18. Ahmad A, Farman M, Naik PA, Hincal E, Iqbal F, Huang Z. Bifurcation and theoretical analysis of a fractional-order Hepatitis B epidemic model incorporating different chronic stages of infection. *J Appl Math Comput.* 2024;71(2):1543-1564. https://doi.org/10.1007/s12190-024-02301-2
19. Evirgen F, Zkse F, Yavuz M, Zdemir N. Real data-based optimal control strategies for assessing the impact of the Omicron variant on heart attacks. *AIMS Bioeng.* 2023;10(3):218-239. https://doi.org/10.3934/bioeng.2023015
20. Evirgen F. Transmission of Nipah virus dynamics under Caputo fractional derivative. *J Comput Appl Math.* 2023;418:114654. https://doi.org/10.1016/j.cam.2022.114654
21. Naik PA, Yeolekar BM, Qureshi S, Yavuz M, Huang Z, Yeolekar M. Fractional Insights in tumor modeling: An interactive study between tumor carcinogenesis and macrophage activation. *Adv Theory Simul.* 2025;8(7). https://doi.org/10.1002/adts.202401477
22. Okundalaye OO, Özdemir N. Harnessing AI for Early Detection and Prediction of Infectious Disease Outbreaks: A Case Study of COVID-19 and Beyond. In: *Systems Science and Nonlinear*

Intelligence Dynamics. WORLD SCIENTIFIC; 2025:183-191.
https://doi.org/10.1142/9789819815432_0017

23. Olaniyi S, Obabiyi OS, Okosun KO, Oladipo AT, Adewale SO. Mathematical modelling and optimal cost-effective control of COVID-19 transmission dynamics. *Eur Phys J Plus.* 2020;135(11).
https://doi.org/10.1140/epjp/s13360-020-00954-z
24. Asamoah JKK, Okyere E, Abidemi A, et al. Optimal control and comprehensive cost-effectiveness analysis for COVID-19. *Results Phys.* 2022;33:105177.
https://doi.org/10.1016/j.rinp.2022.105177
25. Kumar Rai R, Kumar Tiwari P, Khajanchi S. Modeling the influence of vaccination coverage on the dynamics of COVID-19 pandemic with the effect of environmental contamination. *Math Methods in App Sciences.* 2023;46(12):12425-12453.
https://doi.org/10.1002/mma.9185
26. Das T, Bandekar SR, Srivastav AK, Srivastava PK, Ghosh M. Role of immigration and emigration on the spread of COVID-19 in a multipatch environment: a case study of India. *Sci Rep.* 2023;13(1):10546.
https://doi.org/10.1038/s41598-023-37192-z
27. Sharbayta, S. S., Desta, H. D., Abdi, T. Mathematical Modelling of COVID-19 Transmission Dynamics with Vaccination: A Case Study in Ethiopia. *Discrete Dyn Nat Soc.* 2023;2023:1-25.
https://doi.org/10.1155/2023/2972164
28. Rois MA, Fatmawati F, Alfiniyah C. Two isolation treatments on the COVID-19 model and optimal control with public education. *Jambura J Biomath.* 2023;4(1):88-94.
https://doi.org/10.34312/jjbm.v4i1.19963
29. Idisi OI, Yusuf TT, Owolabi KM, Ojokoh BA. A bifurcation analysis and model of Covid-19 transmission dynamics with post-vaccination infection impact. *Healthcare Analytics.* 2023;3:100157.
https://doi.org/10.1016/j.health.2023.100157
30. Shen ZH, Chu YM, Khan MA, Muhammad S, Al-Hartomy OA, Higazy M. Mathematical modeling and optimal control of the COVID-19 dynamics. *Results Phys.* 2021;31:105028.
https://doi.org/10.1016/j.rinp.2021.105028
31. Ullah S, Khan MA. Modeling the impact of non-pharmaceutical interventions on the dynamics of novel coronavirus with optimal control analysis with a case study. *Chaos Soliton Fract.* 2020;139:110075.
https://doi.org/10.1016/j.chaos.2020.110075
32. Khan MA, Atangana A, Alzahrani E, Fatmawati. The dynamics of COVID-19 with quarantined and isolation. *Adv differ equ.* 2020;2020(1):425.
https://doi.org/10.1186/s13662-020-02882-9
33. Asamoah JKK, Owusu MA, Jin Z, Oduro FT, Abidemi A, Gyasi EO. Global stability and cost-effectiveness analysis of COVID-19 considering the impact of the environment: using data from Ghana. *Chaos Soliton Fract.* 2020;140:110103.
https://doi.org/10.1016/j.chaos.2020.110103
34. Péni T, Csutak B, Szederkényi G, Röst G. Nonlinear model predictive control with logic constraints for COVID-19 management. *Nonlinear Dyn.* 2020;102(4):1965-1986.
https://doi.org/10.1007/s11071-020-05980-1
35. Matouk AE. Complex dynamics in susceptible-infected models for COVID-19 with multi-drug resistance. *Chaos Soliton Fract.* 2020;140:110257.
https://doi.org/10.1016/j.chaos.2020.110257
36. Sun D, Duan L, Xiong J, Wang D. Modeling and forecasting the spread tendency of the COVID-19 in China. *Adv differ equ.* 2020;2020(1):489.
https://doi.org/10.1186/s13662-020-02940-2
37. Alshammari FS. A mathematical model to investigate the transmission of COVID-19 in the Kingdom of Saudi Arabia. *Comput Math Methods Med.* 2020;2020:1-13.
https://doi.org/10.1155/2020/9136157
38. Kumar P, Erturk VS, Murillo-Arcila M. A new fractional mathematical modelling of COVID-19 with the availability of vaccine. *Results Phys.* 2021;24:104213.
https://doi.org/10.1016/j.rinp.2021.104213
39. Acuna-Zegarra, MA, Diaz-Infante S, Baca-Carrasco D, Olmos-Liceaga D. COVID-19 optimal vaccination policies: A modeling study on efficacy, natural and vaccine-induced immunity responses. *Math Biosci.* 2021;337:108614.
https://doi.org/10.1016/j.mbs.2021.108614
40. Asamoah JKK, Bornaa CS, Seidu B, Jin Z. Mathematical analysis of the effects of controls on transmission dynamics of SARS-CoV-2. *Alex Eng J.* 2020;59(6):5069-5078.
https://doi.org/10.1016/j.aej.2020.09.033
41. Gatyeni SP, Chukwu CW, Chirove F, Nyabadza F. (Application of optimal control to the dynamics of COVID-19 disease in South Africa. *Scientific African.* 2022;16:e01268.
https://doi.org/10.1016/j.sciaf.2022.e01268
42. Abidemi A, Zainuddin ZM, Aziz NA. B. Impact of control interventions on COVID-19 population dynamics in Malaysia: a mathematical study. *Eur Phys J Plus.* 2021;136(2).
https://doi.org/10.1140/epjp/s13360-021-01205-5
43. Iyaniwura SA, Musa R, Kong JD. A generalized distributed delay model of COVID-19: An endemic model with immunity waning. *Math Biosci Eng.* 2023;20(3):5379-5412.
https://doi.org/10.3934/mbe.2023249
44. Sepulveda G, Arenas AJ, Gonzalez-Parra G. Mathematical Modeling of COVID-19 Dynamics under Two Vaccination Doses and Delay Effects. *Math.* 2023;11(2):369.
https://doi.org/10.3390/math11020369

45. Nisar KS, Farman M, Jamil K, Akgul A, Jamil S. Computational and stability analysis of Ebola virus epidemic model with piecewise hybrid fractional operator. *PLoS ONE.* 2024;19(4):e0298620. https://doi.org/10.1371/journal.pone.0298620
46. Shen X. Applications of fractional calculus in chemical engineering. *uO Research (University of Ottawa).* 2018. https://doi.org/10.20381/ruor-21845
47. Ali MF, Sharma M, Jain R. An application of fractional calculus in electrical engineering. *Adv Eng Technol Appl.* 2016;5(2):41-45. https://doi.org/10.18576/aeta/050204
48. Baleanu D, Kumar D, eds. Fractional Calculus and its Applications in Physics. *Frontiers Research Topics*. 2019. https://doi.org/10.3389/978-2-88945-958-2
49. Magin RL. Fractional calculus in bioengineering: A tool to model complex dynamics. In: *Proceedings of the 13th International Carpathian Control Conference (ICCC).* IEEE; 2012:464-469. https://doi.org/10.1109/carpathiancc.2012.6228688
50. Nisar KS, Anusha C, Ravichandran C, Sabarinathan S. Qualitative analysis on existence and stability of nonlinear fractional dynamic equations on time scales. *Nonlinear Eng.* 2025;14(1):20250150. https://doi.org/10.1515/nleng-2025-0150
51. Ahmad A, Atta U, Akgul A, Sattar S, Ahmad MO. A study on mathematical modeling and control of leptospirosis transmission dynamics during a hurricane with asymptomatic measures. *Modeling Earth Sys Envir.* 2025;11(5). https://doi.org/10.1007/s40808-025-02508-7
52. Tajadodi H, Khan A, Francisco Gomez-Aguilar J, Khan H. Optimal control problems with Atangana-Baleanu fractional derivative. *Opti Contr Appl Meth.* 2020;42(1):96-109. https://doi.org/10.1002/oca.2664
53. Kouidere A, Youssoufi LE, Ferjouchia H, Balatif O, Rachik M. Optimal Control of Mathematical modeling of the spread of the COVID-19 pandemic with highlighting the negative impact of quarantine on diabetics people with Cost-effectiveness. *Chaos Soliton Fract.* 2021;145:110777. https://doi.org/10.1016/j.chaos.2021.110777
54. Ullah R, Waseem M, Rosli NB, Kafle J. Analysis of COVID-19 Fractional model pertaining to the Atangana-Baleanu-Caputo Fractional derivatives. *J Funct Spaces.* 2021;2021:1-16. https://doi.org/10.1155/2021/2643572
55. Joshi H, Jha BK, Yavuz M. Modelling and analysis of fractional-order vaccination model for control of COVID-19 outbreak using real data. *Math Biosci Eng.* 2022;20(1):213-240. https://doi.org/10.3934/mbe.2023010
56. Farman M, Besbes H, Nisar KS, Omri M. Analysis and dynamical transmission of Covid-19 model by using Caputo-Fabrizio derivative. *Alex Eng J.* 2023;66:597-606. https://doi.org/10.1016/j.aej.2022.12.026
57. Ma W, Ma N, Dai C, Chen Y, Wang X. Fractional modeling and optimal control strategies for mutated COVID-19 pandemic. Math Meth Appl Sci. 2023;48(7):7767-7791. https://doi.org/10.1002/mma.9313
58. Ma N, Ma W, Li Z. Multi-Model Selection and Analysis for COVID-19. Fractal and Fractional. 2021;5(3):120. https://doi.org/10.3390/fractalfract5030120
59. Ma W, Zhao Y, Guo L, Chen Y. Qualitative and quantitative analysis of the COVID-19 pandemic by a two-side fractional-order compartmental model. ISA Transactions. 2022;124:144-156. https://doi.org/10.1016/j.isatra.2022.01.008
60. Xu C, Pang Y, Liu Z, Shen J, Liao M, Li P. Insights into COVID-19 stochastic modelling with effects of various transmission rates: simulations with real statistical data from UK, Australia, Spain, and India. Physica Scripta. 2024;99(2):025218. https://doi.org/10.1088/1402-4896/ad186c
61. Rihan, F. A., Udhayakumar, K., Sottocornola, N., Anwar, M. N., Khaliq, A. Q. Stability and Bifurcation Analysis of the Caputo Fractional-Order Asymptomatic COVID-19 Model with Multiple Time-Delays. International Journal of Bifurcation and Chaos. 2023;33(02). https://doi.org/10.1142/s0218127423500220
62. Rihan FA, Gandhi V. Dynamics and Sensitivity of Fractional-Order Delay Differential Model for Coronavirus (COVID-19) Infection. *Progr Fract Differ Appl.* 2021;7(1):43-61. https://doi.org/10.18576/pfda/070105
63. Padmavathi T, Senthamilselvi S, Santra SS, Govindan V, Altanji M, Noeiaghdam S. Rotational Reaction over Infected Covid-19 on Human Respiratory Tract in the Presence of Soret Effect with Hall Current. *BullISUSerMath.* 2022;40:15-33. https://doi.org/10.26516/1997-7670.2022.40.15
64. Gu Y, Ullah S, Khan MA, Alshahrani MY, Abohassan M, Riaz MB. Mathematical modeling and stability analysis of the COVID-19 with quarantine and isolation. *Results Phys.* 2022;34:105284. https://doi.org/10.1016/j.rinp.2022.105284
65. Dhar B, Sajid M. On improving public health after COVID-19 epidemic: A fractal-fractional mathematical solutions with short memory effect and efficient optimal strategies. *PLoS One.* 2025;20(5):e0321195. https://doi:10.1371/journal.pone.0321195
66. Batool H, Khan I, Li W, et al. Fractional modeling and numerical investigations of COVID-19 epidemic model with non-singular fractional derivatives: a case study. *Sci Rep.* 2025;15(1):13256. https://doi.org/10.1038/s41598-025-93095-1

67. Hu R, Aziz MHN, Aruchunan E, Mohamed NA. Modeling and analysis of a delayed fractional order COVID-19 SEIHRM model with media coverage in Malaysia. *Sci Rep.* 2025;15(1):25305. https://doi.org/10.1038/s41598-025-99389-8
68. Sivashankar M, Sabarinathan S, Govindan V, Fernandez-Gamiz U, Noeiaghdam S. (Stability analysis of COVID-19 outbreak using Caputo-Fabrizio fractional differential equation. *AIMS Math.* 2022;8(2):2720-2735. https://doi.org/10.3934/math.2023143
69. Hedayati M, Ezzati R, Noeiaghdam S. New procedures of a fractional order model of novel coronavirus (COVID-19) outbreak via Wavelets Method. *Axioms.* 2021;10(2):122. https://doi.org/10.3390/axioms10020122
70. Sene N. Analysis of the stochastic model for predicting the novel coronavirus disease. *Adv Differ Equ.* 2020;2020(1). https://doi.org/10.1186/s13662-020-03025-w
71. Chatterjee K, Chatterjee K, Kumar A, Shankar S. Healthcare impact of COVID-19 epidemic in India: A stochastic mathematical model. *Medical Journal Armed Forces India.* 2020;76(2):147-155. https://doi.org/10.1016/j.mjafi.2020.03.022
72. Tesfaye AW, Satana TS. Stochastic model of the transmission dynamics of COVID-19 pandemic. *Adv Differ Equ.* 2021;2021(1). https://doi.org/10.1186/s13662-021-03597-1
73. Carriero A, Clark TE, Marcellino M, Mertens E. Addressing COVID-19 Outliers in BVARs with Stochastic Volatility. *SSRN Journal.* 2022. https://doi.org/10.2139/ssrn.4103625
74. Alshammari FS, Akyildiz FT, Khan MA, Din A, Sunthrayuth P. A stochastic mathematical model for understanding the COVID-19 infection using real data. *Symmetry.* 2022;14(12):2521. https://doi.org/10.3390/sym14122521
75. Fatmawati Yuliani E, Alfiniyah C, Juga ML, Chukwu CW. On the Modeling of COVID-19 Transmission Dynamics with Two Strains: Insight through Caputo Fractional Derivative. *Fractal Fract.* 2022;6(7):346. https://doi.org/10.3390/fractalfract6070346
76. Tassaddiq A, Qureshi S, Soomro A, Arqub OA, Senol M. Comparative analysis of classical and Caputo models for COVID-19 spread: vaccination and stability assessment. *Fixed Point Theory Algorithm Sci Eng.* 2024;2024(1). https://doi.org/10.1186/s13663-024-00760-7
77. Liu P, Munir T, Cui T, Din A, Wu P. Mathematical assessment of the dynamics of the tobacco smoking model: An application of fractional theory. *AIMS Math.* 2022;7(4):7143-7165. https://doi.org/10.3934/math.2022398
78. Chu YM, Khan MF, Ullah S, Shah SAA, Farooq M, bin Mamat M. Mathematical assessment of a fractional-order vectorhost disease model with the CaputoFabrizio derivative. *Math Meth Appl Sci.* 2022;46(1):232-247. https://doi.org/10.1002/mma.8507
79. Khan T, Ullah R, Zaman G, Alzabut J. A mathematical model for the dynamics of SARS-CoV-2 virus using the Caputo-Fabrizio operator. *Math Biosci Eng.* 2021;18(5):6095-6116. https://doi.org/10.3934/mbe.2021305
80. Atangana A, Baleanu D. New fractional derivatives with nonlocal and non-singular kernel: Theory and application to heat transfer model. *Therm sci.* 2016;20(2):763-769. https://doi.org/10.2298/tsci160111018a
81. Atangana A, Bonyah E, Elsadany A. A fractional order optimal 4D chaotic financial model with Mittag-Leffler law. *Chin J Phys.* 2020;65:38-53. https://doi.org/10.1016/j.cjph.2020.02.003
82. Al-Refai M, Baleanu D. ON AN EXTENSION OF THE OPERATOR WITH MITTAG-LEFFLER KERNEL. *Fractals.* 2022;30(05). https://doi.org/10.1142/s0218348x22401296
83. Atangana A. Modelling the spread of COVID-19 with new fractal-fractional operators: Can the lockdown save mankind before vaccination? *Chaos Soliton Fract.* 2020;136:109860. https://doi.org/10.1016/j.chaos.2020.109860
84. Idrees M, Alnahdi AS, Jeelani MB. Mathematical modeling of breast cancer based on the Caputo Fabrizio Fractal-Fractional derivative. *Fractal Fract.* 2023;7(11):805. https://doi.org/10.3390/fractalfract7110805
85. Ghanbari B, Gmez-Aguilar JF. Analysis of two avian influenza epidemic models involving fractal-fractional derivatives with power and Mittag-Leffler memories. Chaos: *An Interdisciplinary J Nonlinear Sci.* 2019;29(12). https://doi.org/10.1063/1.5117285
86. Anderson DR, Ulness DJ. Newly defined conformable derivatives. *Advances in Dynamical Systems and Applications.* 2015;10(2):109-137.
87. Baleanu D, Fernandez A, Akgul A. On a fractional operator combining proportional and classical differintegrals. *Mathematics.* 2020;8(3):360. https://doi.org/10.3390/math8030360
88. Kongson J, Thaiprayoon C, Sudsutad W. Analysis of a mathematical model for the spreading of the monkeypox virus with constant proportional-Caputo derivative operator. *AIMS Mathematics.* 2025;10(2):4000-4039. https://doi.org/10.3934/math.2025187
89. Ahmed I, Kumam P, Jarad F, Borisut P, Jirakitpuwapat W. On Hilfer generalized proportional fractional derivative. *Advances in Difference Equations.* 2020;2020(1). https://doi.org/10.1186/s13662-020-02792-w
90. Ul Haq I, Ali N, Bariq A, Akgl A, Baleanu D, Bayram M. Mathematical modelling of COVID-19 outbreak using caputo fractional derivative: stability analysis. *Appl math sci eng.* 2024;32(1). https://doi.org/10.1080/27690911.2024.2326982

91. Hanif A, Kashif Butt AI, Ahmad W. Numerical approach to solve Caputo-Fabrizio-fractional model of corona pandemic with optimal control design and analysis. *Math Meth Appl Sci.* 2023;46(8):9751-9782. https://doi.org/10.1002/mma.9085
92. Kumar A, Prakash A, Mehmet Baskonus H. The epidemic COVID-19 model via Caputo Fabrizio fractional operator. *Waves in Random and Complex Media.* 2022;35(4):6230-6244. https://doi.org/10.1080/17455030.2022.2075954
93. Khan MA, Zafar ZUA, Ahmad I, Isa NM, Alzahrani E. Numerical modeling and simulation of stochastic fractional order model for COVID-19 infection in Mittag Leffler kernel. *Sci Rep.* 2025;15(1):33031. https://doi.org/10.1038/s41598-025-18513-w
94. Sinan M, Alharthi NH. Mathematical analysis of Fractal-Fractional mathematical model of COVID-19. *Fractal Fract.* 2023;7(5):358. https://doi.org/10.3390/fractalfract7050358
95. Kubra KT, Ali R. MODELING AND ANALYSIS OF NOVEL COVID-19 UNDER FRACTAL-FRACTIONAL DERIVATIVE WITH CASE STUDY OF MALAYSIA. *Fractals.* 2021;29(01):2150020. https://doi.org/10.1142/s0218348x21500201
96. Jamil S, Naik PA, Farman M, Saleem MU, Ganie AH. Stability and complex dynamical analysis of COVID-19 epidemic model with non-singular kernel of Mittag-Leffler law. *J Appl Math Comput.* 2024;70(4):3441-3476. https://doi.org/10.1007/s12190-024-02105-4
97. Farman M, Akgul A, Sultan M, et al. Numerical study and dynamics analysis of diabetes mellitus with co-infection of COVID-19 virus by using fractal fractional operator. *Sci Rep.* 2024;14(1):16489. https://doi.org/10.1038/s41598-024-60168-6
98. Kubra KT, Ali R, Alqahtani RT, Gulshan S, Iqbal Z. Analysis and comparative study of a deterministic mathematical model of SARS-COV-2 with fractal-fractional operators: a case study. *Sci Rep.* 2024;14(1). https://doi.org/10.1038/s41598-024-56557-6
99. Shah K, Abdeljawad T. Study of a mathematical model of COVID-19 outbreak using some advanced analysis. *Waves in Random and Complex Media.* 2022;36(1):1-18. https://doi.org/10.1080/17455030.2022.2149890
100. Adel W, Gnerhan H, Nisar KS, Agarwal P, El-Mesady A. Designing a novel fractional order mathematical model for COVID-19 incorporating lockdown measures. *Sci Rep.* 2024;14(1). https://doi.org/10.1038/s41598-023-50889-5
101. Akanni JO, Fatmawati Ajao S, Asamoah JKK, Abimbade SF. Mathematical model of COVID-19 dynamics in the presence of multiple controls. *Qual Quant.* 2024;59(S1):261-290. https://doi.org/10.1007/s11135-024-01975-x
102. Bhatter S, Kumawat S, Purohit SD, Suthar DL. Mathematical modeling of tuberculosis using Caputo fractional derivative: a comparative analysis with real data. *Sci Rep.* 2025;15(1). https://doi.org/10.1038/s41598-025-97502-5
103. Ulam SM. *A Collection of Mathematical Problems.* Interscience Publishers; 1960.
104. Ulam SM. *Problems in Modern Mathematics.* John Wiley & Sons; 1964.
105. Diekmann O, Heesterbeek JAP, Roberts MG. The construction of next-generation matrices for compartmental epidemic models. *J R Soc Interface.* 2009;7(47):873-885. https://doi.org/10.1098/rsif.2009.0386
106. Ahmad A, Atta U, Farman M, Nisar KS, Ahmad H, Hincal E. Investigation of lassa fever with relapse and saturated incidence rate: mathematical modeling and control. *Modeling Earth Sys and Envir.* 2025;11(3). https://doi.org/10.1007/s40808-025-02370-7
107. Atangana A, Araz SI. *New Numerical Scheme With Newton Polynomial: Theory, Methods, and Applications.* Academic Press; 2021. https://doi.org/10.1016/C2020-0-02711-8

Kottakkaran Sooppy Nisar *is a Professor of Mathematics in the Department of Mathematics, College of Science and Humanities, at Prince Sattam bin Abdulaziz University, Al-Kharj, Saudi Arabia. His research interests include fractional-order calculus, biomathematics, fuzzy fractional differential equations, and many related areas.*

https://orcid.org/0000-0001-5769-4320

Muhammad Farman *did Ph.D. Mathematics from the University of Lahore in 2019, Pakistan, and a Postdoc fellowship from Universitas Airlangga Indonesia, Lebanese American University, and Near East University, North Cyprus, Turkey. Adjunct Professor (Research), at Universitas Airlangga Indonesia and University of Lahore, Pakistan. Currently, he is working as an Associate Professor Dr. at Near East University. He has more than eight years of teaching and research experience. The research field is Mathematical biology, Control theory, Numerical Analysis, and Application of fractional calculus on Epidemic models. He published more than three hundred research papers in well-reputed SCI and Scopus journals and presented his work at several national and international conferences. He is the winner of several awards, such as the Research Excellent Awards (Best Researcher of the University), in 2019 and 2020 at the University of Lahore. Stanford University's Top 2% Scientists of 203, 2024 in Applied Mathematics. Best Academic Performance Award 2024, Publication Honorary Award 2024, Most Impactful Researcher Award 2024, Near East University, 2024.*

https://orcid.org/0000-0001-7616-0500

Khadija Jamil *is a research scholar in mathematics at the International Center for Interdisciplinary Research in Sciences, The University of Lahore, Lahore, Punjab, Pakistan. Her research interests include fractional-order calculus, biomathematics, fuzzy fractional differential equations, and many related areas.*
https://orcid.org/0009-0009-3775-9620

Muhammad Kamran *is a Postdoctoral Fellow at Shenzhen University, China. His research focuses on fuzzy mathematics, supply chain management, and sustainability.*
https://orcid.org/0009-0000-5467-0497

An International Journal of Optimization and Control: Theories & Applications
(https://accscience.com/journal/ijocta)